Bone marrow monocytes sustain NK cell-poiesis during non-alcoholic steatohepatitis

Elsa Bourayou, Thibaut Perchet, Sylvain Meunier, Hugo Bouvier, Marie-Pierre Mailhe, Evie Melanitou, Ana Cumano, Rachel Golub

▶ **To cite this version:**

Elsa Bourayou, Thibaut Perchet, Sylvain Meunier, Hugo Bouvier, Marie-Pierre Mailhe, et al.. Bone marrow monocytes sustain NK cell-poiesis during non-alcoholic steatohepatitis. Cell Reports, 2024, 43 (1), pp.113676. 10.1016/j.celrep.2024.113676 . pasteur-04397697

HAL Id: pasteur-04397697
https://pasteur.hal.science/pasteur-04397697

Submitted on 16 Jan 2024

HAL is a multi-disciplinary open access archive for the deposit and dissemination of scientific research documents, whether they are published or not. The documents may come from teaching and research institutions in France or abroad, or from public or private research centers.

L'archive ouverte pluridisciplinaire **HAL**, est destinée au dépôt et à la diffusion de documents scientifiques de niveau recherche, publiés ou non, émanant des établissements d'enseignement et de recherche français ou étrangers, des laboratoires publics ou privés.

Distributed under a Creative Commons Attribution - NonCommercial - NoDerivatives 4.0 International License

Cell Reports

Article

Bone marrow monocytes sustain NK cell-poiesis during non-alcoholic steatohepatitis

Graphical abstract

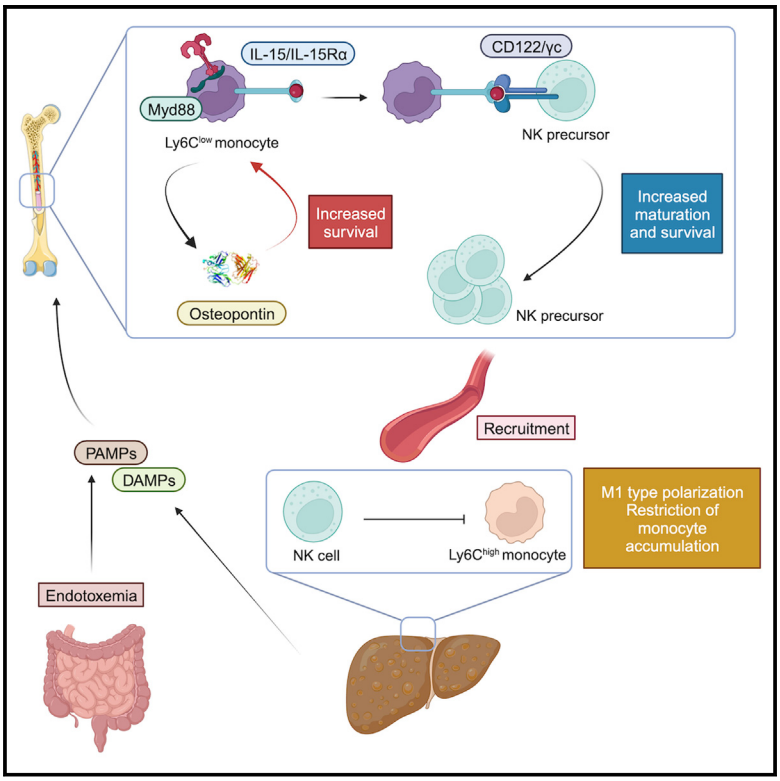

Authors

Elsa Bourayou, Thibaut Perchet, Sylvain Meunier, ..., Evie Melanitou, Ana Cumano, Rachel Golub

Correspondence

rachel.golub@pasteur.fr

In brief

Bourayou et al. demonstrate that, during NASH, endotoxemia-derived signals activate medullary monocytes, which upregulate both the IL-15/IL-15Rα complex and osteopontin, promoting NK precursor maturation and survival. These NK precursors exit the bone marrow and join the liver, where they dampen fibrogenesis and polarize recruited monocytes toward an M1-like phenotype.

Highlights

- Endotoxemia promotes IL-15/IL-15Rα and osteopontin expressions in medullary monocytes
- The NK cell/monocyte dialogue enhances NK precursor maturation and survival
- NK precursors recirculate and are recruited to the liver
- Liver NK cells limit fibrogenesis and polarize monocytes

Bourayou et al., 2024, Cell Reports *43*, 113676
January 23, 2024 © 2024 The Authors.
https://doi.org/10.1016/j.celrep.2024.113676

CellPress

Cell Reports

CellPress
OPEN ACCESS

Article

Bone marrow monocytes sustain NK cell-poiesis during non-alcoholic steatohepatitis

Elsa Bourayou,[1] Thibaut Perchet,[1,4] Sylvain Meunier,[1,2,4] Hugo Bouvier,[1] Marie-Pierre Mailhe,[1] Evie Melanitou,[3] Ana Cumano,[1] and Rachel Golub[1,5,*]

[1]Institut Pasteur, Université Paris Cité, INSERM U1223, Lymphocyte and Immunity Unit, 75015 Paris, France
[2]Institut Mondor de Recherche Biomédicale (IMRB), INSERM U955, 94000 Créteil, France
[3]Institut Pasteur, Université Paris Cité, Department of Parasites and Insect Vectors, 75015 Paris, France
[4]These authors contributed equally
[5]Lead contact
*Correspondence: rachel.golub@pasteur.fr
https://doi.org/10.1016/j.celrep.2024.113676

SUMMARY

Natural killer (NK) cells are the predominant lymphocyte population in the liver. At the onset of non-alcoholic steatohepatitis (NASH), an accumulation of activated NK cells is observed in the liver in parallel with inflammatory monocyte recruitment and an increased systemic inflammation. Using *in vivo* and *in vitro* experiments, we unveil a specific stimulation of NK cell-poiesis during NASH by medullary monocytes that trans-present interleukin-15 (IL-15) and secrete osteopontin, a biomarker for patients with NASH. This cellular dialogue leads to increased survival and maturation of NK precursors that are recruited to the liver, where they dampen the inflammatory monocyte infiltration. The increase in the production of both osteopontin and the IL-15/IL-15Rα complex by bone marrow monocytes is induced by endotoxemia. We propose a tripartite gut-liver-bone marrow axis regulating the immune population dynamics and effector functions during liver inflammation.

INTRODUCTION

In Western countries, where unbalanced diets are causing a rise in obesity and metabolic disease incidence, the prevalence of non-alcoholic fatty liver diseases (NAFLDs) is now skyrocketing. NAFLDs are a spectrum of hepatic diseases ranging from simple steatosis to severe stages such as non-alcoholic steatohepatitis (NASH) and cirrhosis and can further evolve into hepatocellular carcinoma (HCC).[1] Yet, the pathogenesis of the different stages and why some patients progress toward fibrosis and/or HCC are still not fully known. There is a need to further understand the cellular and molecular events underlying NASH evolution.

The contributions of lymphocytes to NASH have been broadly studied,[2,3] and natural killer (NK) cells were shown to be involved in the disease progression.[4–9] NK cells are part of the type 1 innate lymphoid cell (ILC1) subset, thus sharing characteristics with ILC1s. Both ILC1s and NK cells produce type 1 cytokines such as interferon γ (IFNγ) and tumor necrosis factor α (TNF-α) upon activation by interleukin-12 (IL-12), IL-18, or IL-15. NK cells rely on the expression of the T-box transcription factors T-BET and eomesodermin (EOMES), while ILC1s only express T-BET.[10] NK cells and liver ILC1s also exhibit cytotoxic activities with the expression of TNF-related apoptosis-inducing ligand (TRAIL) as well as granzyme B (GzmB) and perforin.[11,12] In the liver, NK and ILC1s represent 30%–50% of total lymphocytes in humans and around 10% in mice, and the liver contains both ILC1 precursors (ILC1Ps) and mature ILC1s.[13,14] Murine NASH models are obtained by feeding mice with specific diets to induce fatty liver, causing inflammation and injuries. In the latter, hepatic NK cell numbers significantly increase. In liver injury, NK cells have been shown to play an anti-fibrotic role by killing hepatic stellate cells (HSCs)[15,16] and by polarizing macrophages toward an M1 profile.[4,5] This suggests a protective role for these cells that keeps the disease from progressing toward more severe stages. Yet, another study showed that NK cells can play a detrimental role by promoting NASH progression via enhanced cytokine production and JAK/STAT-mediated hepatocyte damages.[6] Thus, NK cells' role in NASH remains unclear. Moreover, the mechanisms underlying the increased hepatic NK cell pool were never addressed. Another major immune population involved in NASH establishment is the monocytes/macrophages. Liver myeloid populations represent a highly heterologous population[17–19] and were shown to play multiple roles in NASH pathogenesis.[20,21]

Using different NASH-inducing diets in murine models, we show that NK cells are recruited to the liver, where they restrict Ly6C^{high} monocyte recruitment and polarize them toward an M1 phenotype. Looking at the bone marrow (BM), where NK cell development takes place, we observed enhanced NK cell-poiesis along with increased IL-15-dependent survival and maturation of NK precursors in diet-induced (DI)-NASH. In BM monocytes, both IL-15/IL-15Rα complex and osteopontin (OPN) expressions were upregulated. Using *in vitro* co-cultures of BM monocytes with NK precursors, we were able to

This is an open access article under the CC BY-NC-ND license (http://creativecommons.org/licenses/by-nc-nd/4.0/).

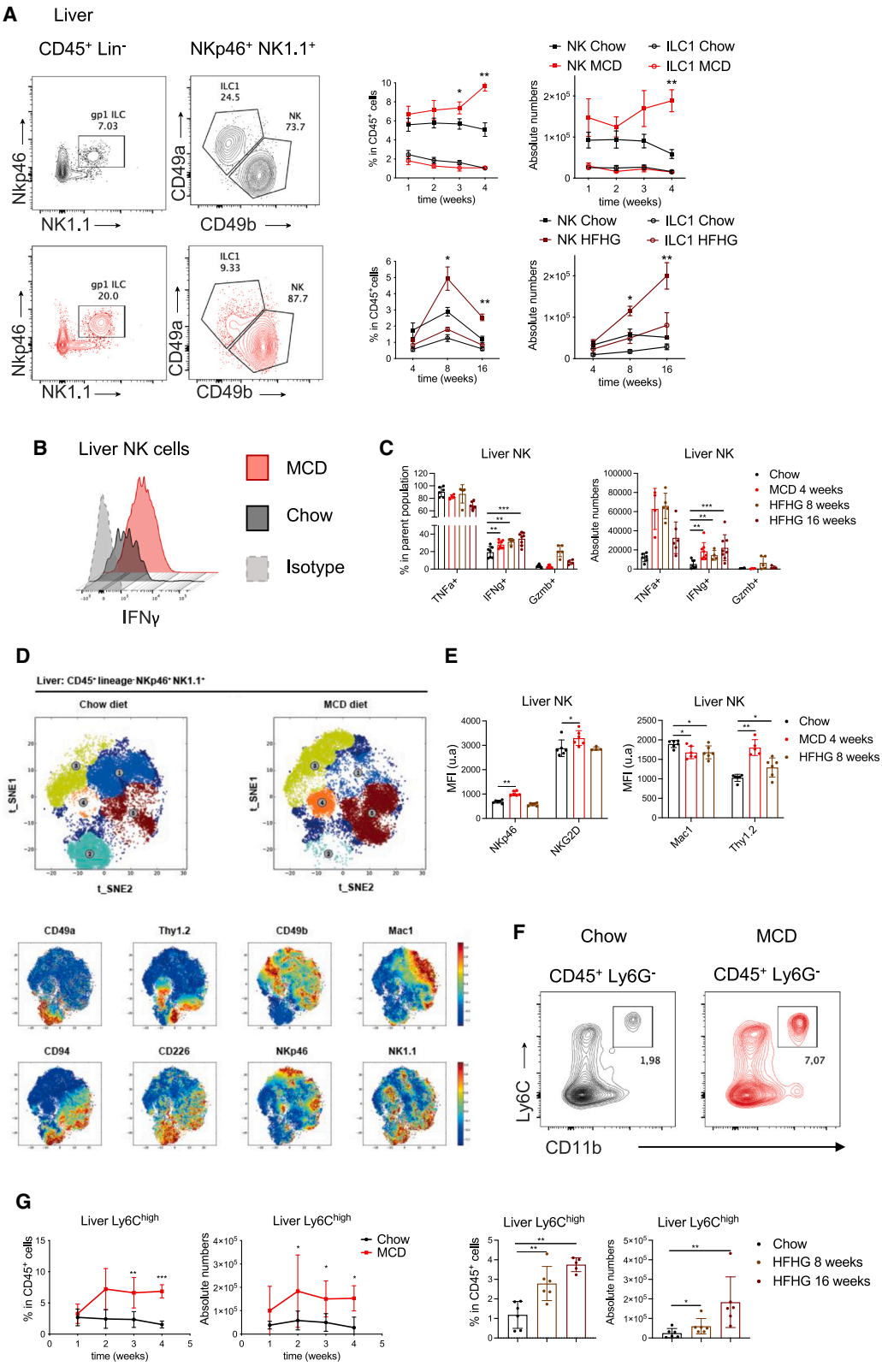

(legend on next page)

demonstrate that the former can directly promote NK cell maturation and survival through IL-15/IL-15Rα trans-presentation and OPN secretion. Lastly, we showed that myeloid differentiation factor 88 (Myd88)-dependent pathogen-associated molecular pattern (PAMP) signaling was responsible for the increased production of both the IL-15/IL-15Rα complex and OPN by medullary monocytes. Together, our data reveal an endotoxemia-driven crosstalk between monocytes and NK precursors in the BM that favors NK cell development and sustains their recruitment to the liver during DI-NASH. We also unveil a role for OPN as one of the key molecules involved in the NK cell/monocyte dialogue and thus regulating their immune response during inflammation.

RESULTS

Both liver ILC1s and myeloid populations are impacted by DI-NASH

We chose to compare complementary nutritional mouse models of NASH. The methionine- and choline-deficient (MCD) diet induces liver dyslipidemia and inflammation with massive hepatocyte damage due to lipid accumulation in hepatocytes and, eventually, liver fibrosis. The cholesterol-enriched high-fat, high-glucose (HFHG) diet reproduces some human metabolic dysfunctions associated with obesity (hyperinsulinemia and hyperglycemia) on top of liver inflammation. As expected, both diets induce strong steatosis confirmed by oil red O staining after 4 and 8 weeks, respectively, for the MCD and HFHG diets (Figure S1A). Serum alanine aminotransferase (ALT) and aspartate aminotransferase (AST) are elevated (Figure S1B). Cholesterol levels are significantly increased in the HFHG but not in the MCD diet, while serum triglyceride levels are decreased (Figure S1C). Quantitative real-time PCR (real-time qPCR) on liver tissue samples from mice fed with MCD or HFHG diet revealed the upregulation of genes involved in inflammation (*Tnf*, *Il1b*) and fibrogenesis (*Col1a1*, *Timp*, *Acta2*), reflecting liver damage (Figure S1D). Mice fed under the HFHG diet possess a significant increase in both body and liver weight (Figure S1E) promoting the associated metabolic syndromes: obesity and insulin resistance (Figure S1F).

Using flow cytometry, we analyzed the hepatic ILC1 compartment during DI-NASH. Liver NK cells, but not ILC1s, are significantly increased in frequency and absolute numbers as soon as after 3 weeks of MCD diet and 8 weeks of HFHG diet compared to mice fed with a control (chow) diet (Figure 1A). This rise is accompanied by a significant increase in IFNγ production by NK cells in both NASH diets, while the frequency and numbers of TNF-α^+ and GzmB$^+$ NK cells do not vary (Figures 1B and 1C). Using a t-distributed stochastic neighbor embedding (t-SNE) analysis based on the differential expression of 14 surface markers, including 10 expressed by ILC1s, we discriminate 5 main clusters. Cluster 2 represents ILC1s, while NK cells are shared among 4 clusters depending on the expression level of several markers. Notably, an enrichment in clusters 3, 4, and 5 occurred in the MCD diet (Figure 1D). The activating receptors (NKp46, NKG2D) are upregulated on the NK cell surface in MCD-induced NASH (Figure 1E). The maturation marker CD11b is downregulated in both DI-NASH diets (Figure 1E). Thy1.2 expression was also increased on MCD-diet- and 8 week HFHG-diet-derived NK cells compared to their control counterparts (Figures 1D and 1E).

The cytotoxic CD8$^+$ T cells were increased in both frequency and absolute numbers in DI-NASH liver, while helper CD4$^+$ T cells remained unchanged (Figure S2A). Inflammatory monocytes defined as Ly6G$^-$Ly6C^{high}CD11b$^+$ cells were recruited to the liver, with a significant difference starting after 2 weeks of MCD diet and after 8 weeks of HFHG diet compared to chow diet (Figures 1F and 1G).

In conclusion, both liver monocytes and NK cell populations increase in frequency and absolute numbers in DI-NASH. The latter display an activated phenotype with the upregulation of NK cell receptors such as NKp46 and NKG2D as well as an enhanced secretion of the pro-inflammatory cytokine IFNγ.

NK cells protect the liver against the priming of fibrogenesis while restricting inflammatory Ly6C^{high} monocyte recruitment

To determine the role of NK cells in NASH establishment and progression, we used two approaches. One model of depletion based on the anti-asialo(as)GM1 antibody (Figure 2A) and the NK-deficient IL-15-knockout (KO) mouse model. The absence of NK cells was efficient in both models (Figure S2B). Gut Nkp46$^+$ ILC3 (Figure S2C) and liver NK T cell populations (Figure S2D) were not affected by depletion with anti-asGM1. Anti-asGM1-injected mice under MCD diet displayed similar ALT and AST serum levels compared to non-injected, MCD-fed mice (Figure 2B). The fibrosis-related gene program in the liver appeared upregulated in MCD-fed, anti-asGM1-injected mice and IL-15-KO mice compared to their wild-type (WT) counterparts (Figure 2C). *Ccl2*, *Tnf*, and *Il1b* relative mRNA expressions remained unaltered between the anti-asGM1-injected IL-15-KO and non-injected, MCD-fed mice, while those of *Col1a1*, *Acta2*,

Figure 1. Liver type 1 ILCs and monocytes are both impacted by NASH

(A) Flow cytometric analyses and evolution of percentage and numbers of type 1 ILCs from livers of WT mice fed with a chow diet (black) or MCD diet (red) for 4 weeks or HFHG diet (purple) for up to 16 weeks.

(B) Mean fluorescence intensity (MFI) of IFNγ in liver NK cells from chow- or MCD-fed WT mice.

(C) Analyses of hepatic NK cell secretion in MCD-fed (left) and HFHG-fed (right) mice.

(D) t-SNE analyses of liver type 1 ILCs based on differential expression of CD49a, CD49b, CD94, CD226, CD11b, NK1.1, NKp46, and Thy1.2 (top). Relative fluorescence intensities of mentioned surface markers (bottom).

(E) MFI of NK cell surface markers in chow, MCD, and HFHG conditions.

(F and G) Flow cytometric analyses (F) and evolution of percentage and absolute numbers (G) of infiltrating Ly6C^{high} monocytes in livers from mice fed with the different diets.

Data are means ± SD of at least two independent experiments with at least three mice in each condition per experiment. *$p < 0.05$, **$p < 0.01$, ***$p < 0.001$, and ****$p < 0.0001$ by Mann-Whitney test.

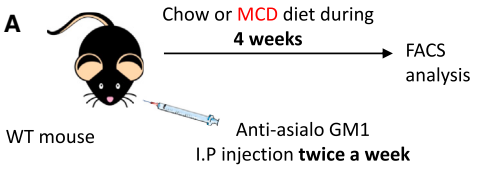

B

	WT		anti-asGM1		IL-15 KO	
	Chow	MCD	Chow	MCD	Chow	MCD
ALT	10,33 ± 8,23	786,05 ± 389,76	22,16 ± 7,49	660,71 ± 467,81	38,33 ± 467,81	310,66 ± 213,42
AST	165,9 ± 85,75	655,16 ± 247,42	61,33 ± 22,74	576,71 ± 242,40	289,75 ± 187,96	362,85 ± 227,76
NAS Score	-	2,69 ± 0,49	-	3,38 ± 0,037	-	3,44 ± 0,78

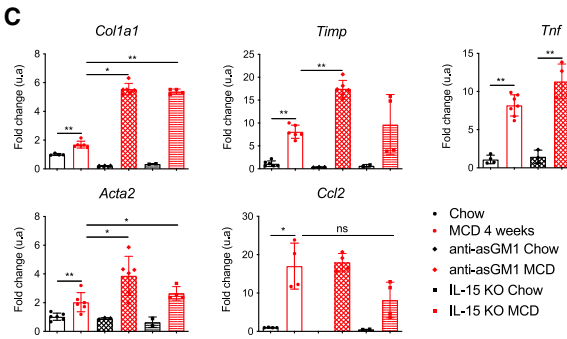

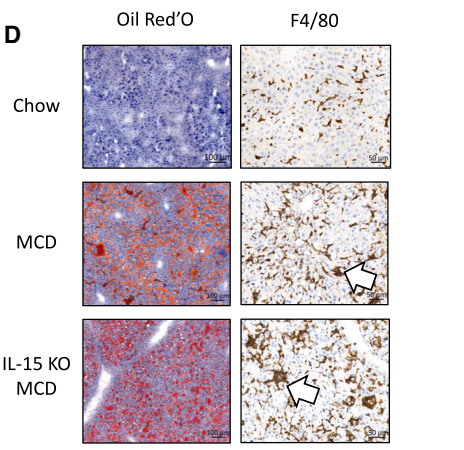

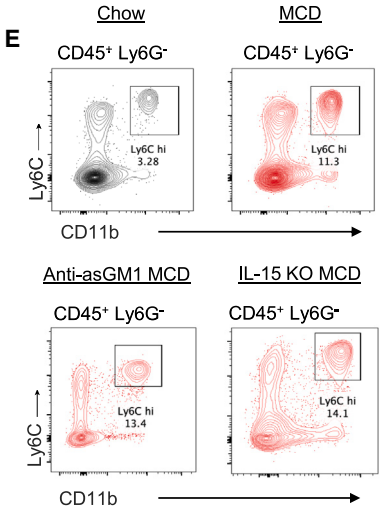

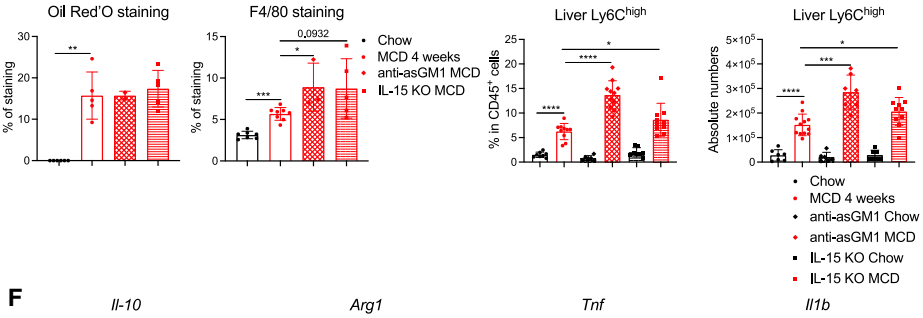

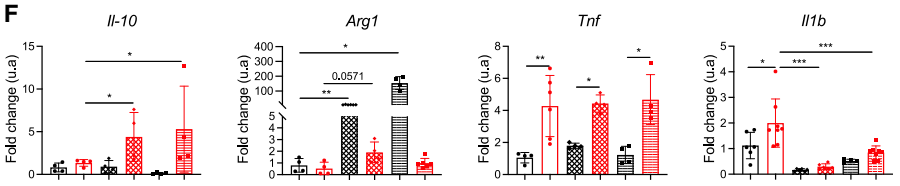

(legend on next page)

and *Timp* (Figure 2C) were significantly increased in the absence of NK cells, suggesting an enhanced pro-fibrogenic environment. Steatosis was not affected by the absence of NK cells, as revealed by quantification of oil red O staining (Figure 2D).

We then performed F4/80 staining on liver sections from anti-asGM1-injected IL-15-KO and non-injected WT mice fed with chow or MCD diet (Figure 2D). Quantification of the F4/80 staining revealed an increase in the absence of NK cells (Figure 2D). This was confirmed by a significant rise in Ly6C^{high} monocyte frequency and numbers in MCD-fed, anti-asGM1-injected and IL-15-KO mice compared to MCD-fed, non-injected WT mice (Figure 2E). This led to an aggravation of the pathology as revealed by a significantly increased NAS in MCD-fed IL-15-KO mice compared to WT mice (Figures 2B and S2E). Monocytes are recruited to the liver via the CCR2/CCL2 axis during DI-NASH.[22] While hepatic CCL2 levels remained unchanged in NK-deficient mice compared to NK-sufficient counterparts, NK cells also express *Ccr2* (Figure S2F). In addition, the frequency of liver Annexin V$^+$ Ly6C^{high} monocytes was significantly reduced in MCD-fed IL-15-KO mice compared to their WT counterparts (Figure S2G), indicating that monocyte accumulation might also rely on a decreased cell death. Liver NK cells displayed an upregulation of *Tnfsf10* (coding for TRAIL) in the NASH diet conditions (Figure S2H), highlighting a potential activation of the TRAIL-dependent cytotoxic pathway in these cells during DI-NASH.

We also performed quantitative real-time PCR on fluorescence-activated cell-sorted (FACS) liver Ly6C^{high} monocytes from the different conditions. The MCD diet promotes an M1-type response with the upregulation of the pro-inflammatory genes *Tnf* and *Il1b* along with the downregulation of the M2 marker gene *Arg1*, coding for arginase 1 (Figure 2F). In MCD-fed, anti-asGM1-injected and IL-15-KO mice, Ly6C^{high} monocyte gene expression was impacted with an upregulation of the anti-inflammatory gene *Il10* and a decrease in *Il1b* expression. *Arg1* was significantly upregulated in chow diet in NK-depleted and -deficient mice compared to NK-sufficient counterparts (Figure 2F). Similar modifications in liver monocyte gene expression were observed in MCD-fed IFNγ-KO mice compared to MCD-fed WT mice (Figure S2I). Indeed, although *Il10* level of expression was not affected by the absence of IFNγ, *Arg1* was significantly upregulated, and *Tnf* and *Il1b* were downregulated. This suggests that liver NK cells promote an M1 phenotype in recruited monocytes and that this process is mediated by IFNγ.

In conclusion, liver NK cells restrict the recruitment of Ly6C^{high} monocytes while maintaining an M1 profile. The priming of liver fibrosis, related to enhanced liver injury, is upregulated in the absence of NK cells, confirming an anti-fibrotic role for these cells in this organ as shown by others.[5,15,16]

Recently proliferating Thy1.2$^+$CD27$^+$ NK cells are recruited to the liver

To investigate the phenomenon responsible for the increase in liver NK cells in DI-NASH, we assessed their proliferation using the Ki67/DAPI staining on livers from chow-, MCD-, or HFHG-fed mice (Figure 3A). Although around 80% of NK cells were in G1 phase, suggesting recent proliferation and cell growth, no significant difference was observed for presumed dividing subsets.

We focused on a possible active recruitment of NK cells to the liver. We compared NK cell frequencies from portal vein blood and circulating blood between diets. NK cell circulation was significantly increased in both MCD and 8 week HFHG diets compared to chow diet, suggesting an active recruitment to the liver (Figures 3B and 3C). This phenomenon disappeared after 16 weeks of HFHG diet (Figures 3B and 3C). Hence, we chose to continue our analyses on early stages of HFHG diet (8 weeks). We observed an enrichment in Thy1.2$^+$CD27$^+$ NK cells in blood and liver in both NASH diets (Figures 3D and 3E). This corroborates the idea that accumulating liver NK cells come from the circulation in DI-NASH.

CXCR3 expression revealed an increase in the percentage of CXCR3$^+$ blood and liver NK cells from MCD- and HFHG-fed mice (Figures 3F and 3G). These CXCR3$^+$ NK cells co-stain for the Thy1.2 marker (Figure 3G). Expressed on activated T and NK cells, CXCR3 binds to IFNγ-inducible ligands: CXCL9, CXCL10, and CXCL11, respectively.[23] *Cxcl9* and *Cxcl11* mRNA relative expressions in liver from MCD-fed mice were upregulated yet showed no difference in HFHG-fed mice (Figure S2J). On the other hand, *Cxcl10* was upregulated in both diets (Figure 3H). This supports the findings of Fan et al. that NK cells are recruited to the liver through the CXCR3/CXCL10 axis during DI-NASH.[4]

Given that CXCL10 induction is downstream of the IFNγ signaling, we postulated that CXCL10 expression and subsequently liver NK cell recruitment would be altered in IFNγ-deficient mice. In MCD-fed IFNγ-KO mice, ALT and AST activities were significantly decreased compared to their WT counterparts (Figure S3A). Absolute numbers of hepatic NK cells significantly dropped in chow- and MCD-fed IFNγ-KO mice in comparison to WT mice (Figure S3B). Yet, the increased accumulation of liver NK cells was proportionally similar, as revealed by fold change normalization (Figure S3B). As for CXCL10 expression, it was not downregulated in IFNγ-KO compared to WT mice nor in chow- or MCD-diet-fed mice (Figure 3I). IFNγ-independent CXCL10 expression in hepatocytes was shown to depend on IRF3 signaling during hepatitis,[24] and activation of the STING/IRF3 pathway promotes hepatocyte inflammation in NASH

Figure 2. NK cells protect the liver against the priming of fibrogenesis while restricting inflammatory Ly6C^{high} monocyte recruitment

(A) Experimental model used for NK cell depletion.

(B) Individual scores and NAFLD Activity Score (NAS). NAS was calculated from individual scores for steatosis, lobular inflammation, and ballooning.

(C) Relative mRNA expression levels of pro-fibrogenic genes by quantitative real-time PCR on liver tissues from mice in different conditions.

(D) Representative images of oil red O (left) and F4/80 (right) staining and quantitative analyses of livers.

(E) Flow cytometric analyses and percentage and absolute numbers of liver Ly6C^{high} monocytes.

(F) mRNA expression levels of genes on FACS liver Ly6C^{high} monocytes.

Data are means ± SD of at least two independent experiments with at least three mice in each condition per experiment. *$p < 0.05$, **$p < 0.01$, ***$p < 0.001$, and ****$p < 0.0001$ by Mann-Whitney test.

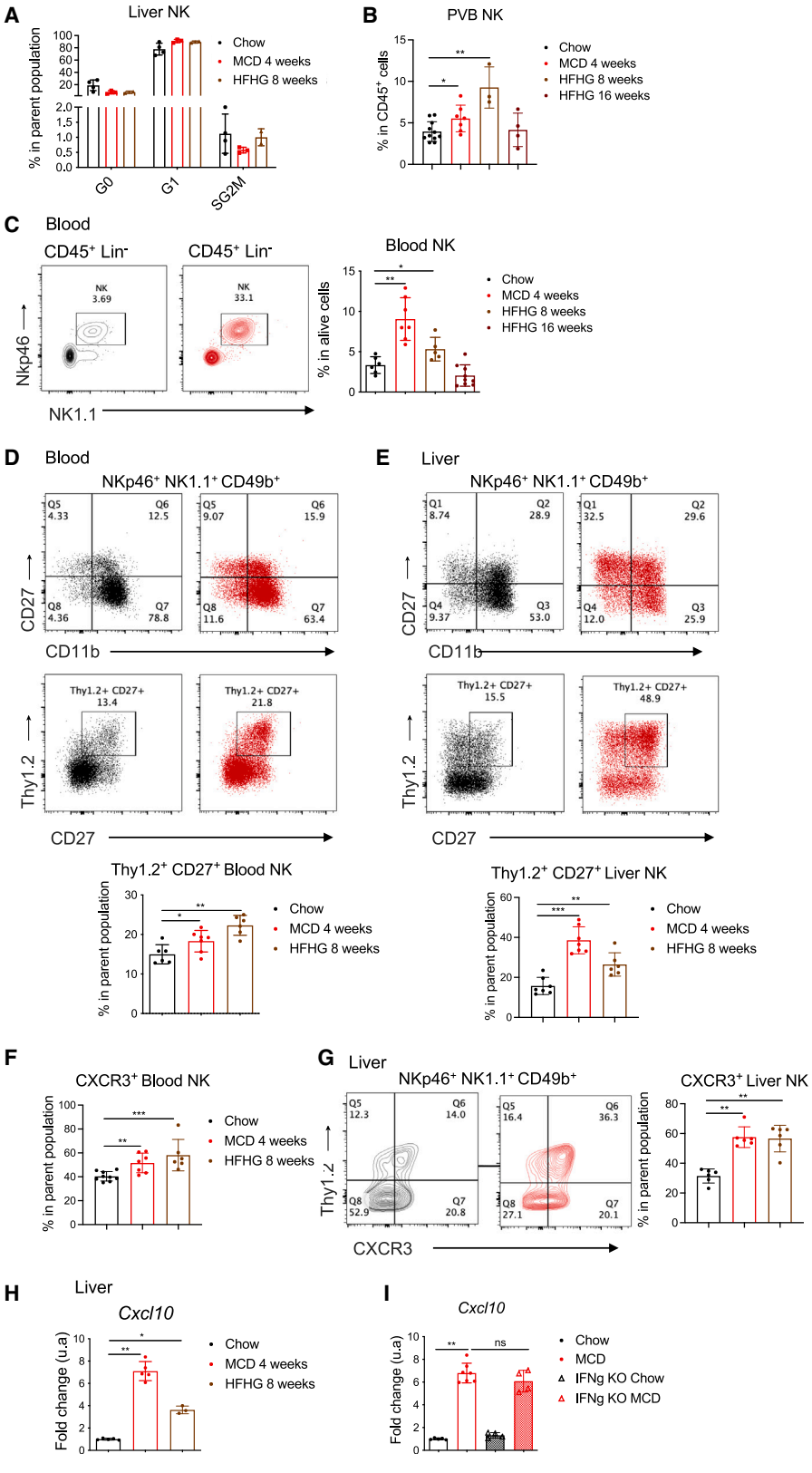

(legend on next page)

mouse models and human liver cell lines.[25] Our results confirm that the CXCR3/CXCL10 axis is IFNγ independent in DI-NASH.

DI-NASH promotes survival and maturation of NK cell progenitors in the BM

We sought to determine the origin of the hepatic-recruited NK cells. In the periphery, both intestine and spleen NK cell numbers are decreased, suggesting their egress (Figure S3C). The enrichment in circulation of Thy1.2$^+$CD27$^+$ NK cells led us to consider the BM as another potential source for this "immature" phenotype of recruited cells. In the BM, the refined NK progenitor (rNKp), characterized by the expression of IL-15Rβ (CD122), gives rise to the immature NK (iNK) cells (Figure 4A). Then, the maturation process could be subdivided based on the relative expression of CD27 and CD11b, with CD27$^+$CD11b$^-$ precursor cells that differentiate into double-positive (DP; Figure 4A) cells and then into the final mature CD27$^-$CD11b$^+$ NK stage.[26] Both DP and CD27$^-$CD11b$^+$ cells can exit the BM, although this depends on the expression of S1pr5.[27] NK cells and ILC1s belong to distinct developmental pathways. ILC1s arise from the common helper innate lymphoid progenitor (CHILP), and ILC1P has been identified within the BM.[28,29]

We observed a significant increase in BM NK progenitor numbers in both NASH diets (Figures 4B and S3D). This is likely the result of increased rNKp proliferation during early onset of the disease as revealed by BrdU experiments and increased survival highlighted by BCL-2 expression (Figure 4B). No difference in iNK numbers was observed (Figure 4C). In contrast, CD27$^+$CD11b$^-$ and DP stages of NK cells showed a significant increase in numbers in both MCD- and HFHG-fed mice (Figures 4C and S3D). Interestingly, while NK progenitors increase in numbers, the total BM immune cellularity decreases in DI-NASH, and other progenitors such as the Lin$^-$Sca-1$^+$c-Kit$^-$ (LSK) cells and the common lymphoid progenitor (CLP) display no difference between diets (Figures S3E and S3F). Similarly, absolute numbers of BM ILC1P decreased in the MCD diet and displayed no significant difference in the HFHG diet compared to chow diet (Figure S3G). Altogether, this suggests that DI-NASH specifically favors NK cell-poiesis.

No proliferative difference could be detected with similar frequency and numbers of BrdU$^+$ CD27$^+$CD11b$^-$ cells (Figure S3H). Since accumulation of NK precursors started at the transition from the iNK to CD27$^+$CD11b$^-$ stage, we FACS a mix of both stages from mice fed with a chow, MCD, or HFHG diet and performed quantitative real-time PCR on genes involved in NK cell maturation and survival. Notably, *Tbx21*, the gene coding for T-BET, essential for NK maturation, as well as its downstream gene, *Blimp1*, were both upregulated in MCD and HFHG diets compared to chow (Figure 4D). Both gene expressions are dependent on IL-15.[30] *Eomes* was also upregulated in both NASH diets (Figure 4D). The expression of the *Klf2* transcript was increased in iNK/CD27$^+$CD11b$^-$ cells from MCD- and HFHG-fed mice compared to their chow-fed counterparts (Figure 4D). KLF2 regulates NK cell maturation via the upregulation of the homing receptor CD62L, thereby dictating their access to IL-15 and their survival in the periphery.[31] Anti-apoptotic *Bcl2* and *Mcl1* are proteins downstream of STAT5, which is itself a target of IL-15 signaling.[32] Their expression is increased in MCD-derived iNK/CD27$^+$CD11b$^-$ cells compared to chow-derived cells (Figure 4D). Similar results were obtained in FACS DP cells from chow-, MCD-, and HFHG-fed mice (Figure S3I).

While EOMES was upregulated at the iNK cell stage, T-BET and BCL-2 levels of expression were increased at the CD27$^+$CD11b$^-$ stage in both NASH diets (Figure 4E). Altogether, these results suggest the upregulation of maturation and survival gene programs via IL-15 signaling in NK precursors during DI-NASH.

Lastly, we assessed Thy1.2 and CXCR3 expression by NK precursors. Both expressions decrease along the developmental pathway, with 70% of CD27$^+$CD11b$^-$ cells being Thy1.2$^+$CXCR3$^+$ and only 15% of CD27$^-$CD11b$^+$ cells being DP (Figure 4F). CXCR3 expression was upregulated on all NK precursors in both MCD and HFHG compared to chow diet (Figure 4F). *S1pr5* expression was increased in CD27$^+$CD11b$^-$ and DP cells from MCD- and HFHG-fed mice (Figure 4G). This suggests that circulating and recruited liver NK cells originate from the BM and that NK cells leave at the CD27$^+$CD11b$^-$ and DP stages along with the mature CD27$^-$CD11b$^+$ stage.

In conclusion, DI-NASH promotes NK cell-poiesis via an expansion of proliferating rNKp cells as well as via an accumulation of NK precursors in the BM that then likely enter the circulation.

BM Ly6C^{low} monocytes positively regulate NK cell maturation and survival during DI-NASH via IL-15 trans-presentation and OPN secretion

We performed mixed BM chimera experiments to check whether the upregulation of survival and maturation gene programs of NK precursors was cell intrinsic. CD45.2$^+$ immune BM progenitors from WT mice under chow diet were mixed at a 1:1 ratio with GFP$^+$ immune BM progenitors under MCD diet and injected into irradiated CD45.1$^+$ Ragγc-deficient hosts fed either with chow or MCD diets (Figure S4A). Liver and BM analyses revealed NK precursor and liver NK cell accumulation in MCD- compared to chow-fed hosts (Figures S4B–S4E). The chimerism was

Figure 3. Recently proliferating Thy1.2$^+$CD27$^+$ NK cells are actively recruited to the liver

(A) Percentage in parent population of NK cells in G0, G1, and SG2M phases performed by KI-67/DAPI staining in liver from mice fed with chow, MCD, and HFHG diets.

(B) Frequencies of portal vein blood (PVB) NK cells from chow-, MCD-, and HFHG-fed mice.

(C) Flow cytometric analyses (left) and frequencies of blood NK cells.

(D and E) Flow cytometric analyses and frequencies in parent populations of blood (D) and liver (E) Thy1.2$^+$ CD27$^+$ NK cells in chow, MCD, and HFHG diets.

(F and G) Frequencies of CXCR3$^+$ NK cells in blood (F) and livers (G) from mice fed with chow, MCD, or HFHG diets.

(H and I) Relative mRNA expression levels of *Cxcl10* in liver tissues from WT mice (H) and IFNγ-KO mice (I) fed with the different diets.

Data are means ± SD of at least two independent experiments with at least three mice in each condition per experiment. *p < 0.05, **p < 0.01, ***p < 0.001, and ****p < 0.0001 by Mann-Whitney test.

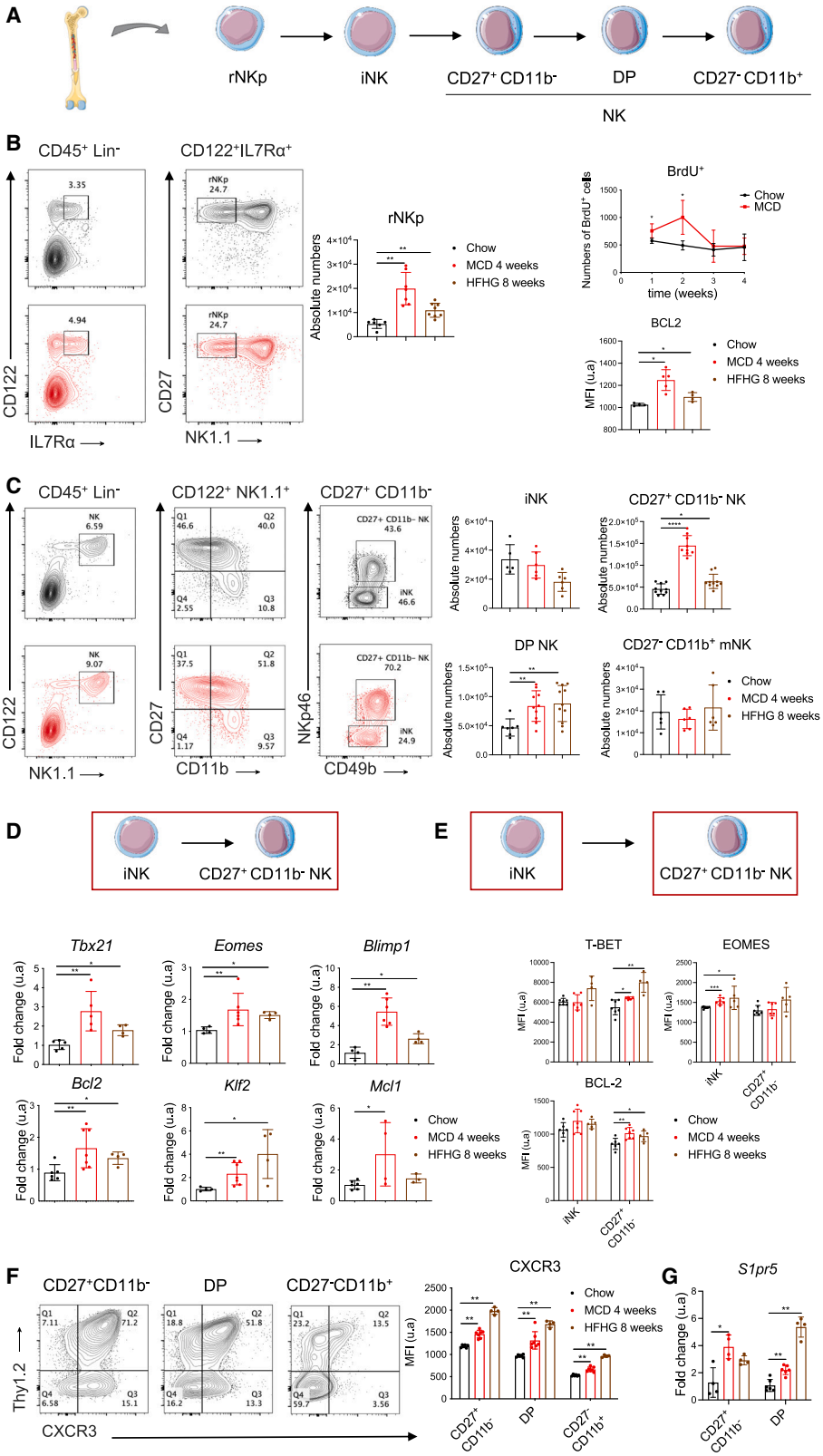

(legend on next page)

around 50% in NK precursors and hepatic NK cells, demonstrating that the enhanced maturation and functional response of NK cells in DI-NASH entirely relies on environmental cues and does not imprint the progenitor pool.

We focused on inflammatory cytokines and adipokines known for their implication in DI-NASH. Using the multiplex assay Luminex technique, we measured their levels in BM supernatants. Most cytokine levels were below the detection threshold except for IL-33, for which levels significantly dropped in DI-NASH compared to chow diet (Figure S5A). Soluble levels of IL-15 remained unaltered (Figure S5A). Leptin and adiponectin displayed no clear difference apart from a rise in leptin concentration in the 8 week HFHG diet (Figure S5A). In contrast, we observed a significant increase in OPN concentration in both NASH diets (Figure 5A). OPN can be produced by BM stromal cells.[33,34] BM CD45$^-$CD31$^-$Sca-1$^-$PDGFRβ$^+$ stromal cells displayed an increase in *Spp1* expression in the MCD diet but no upregulation of the *Il15* and *Il15Ra* genes (Figure S5B). Hepatic monocytes and macrophages were previously described as possible producers of OPN in DI-NASH.[17] In NASH diets, the BM Ly6C^{low} subset showed an increase in frequency and in numbers (Figure 5B). We performed quantitative real-time PCR on FACS monocytes (Figure S5C) to assess the levels of expression of *IL15*, *Il15Ra*, and *Spp1* in the different diets. *Il15* and *Spp1* genes were significantly upregulated in MCD- and HFHG-derived BM Ly6C^{low} monocytes (Figure 5C). Two isoforms of OPN exist: one intracellular (iOPN) and another secreted (sOPN).[35] Cultures of MCD-derived Ly6C^{low} monocytes showed a rise in OPN concentration in supernatants, demonstrating that they increase its secretion (Figure 5D).

To elucidate whether BM monocytes play a role in NK cell maturation and survival in DI-NASH, we performed 5 day co-cultures of BM Ly6C^{low} monocytes from WT, OPN-KO, or IL-15-KO mice with CD27$^+$CD11b$^-$ NK cells from WT mice or single cultures of WT CD27$^+$CD11b$^-$ NK cells (Figure 5E). Levels of *Spp1* were significantly increased in monocytes after 5 days of culture, while *Il15* and *Il15Ra* levels of expression were not impacted (Figure S5D). Moreover, during the 5 days of culture, T-BET, EOMES, and CD11b expressions remarkably increase, indicating that NK precursors differentiate (Figures S5E and S5F). All T-BET, EOMES, and BCL-2 expressions were significantly increased in co-cultures with WT and OPN-KO monocytes compared to single cultures (Figure 5F). However, all three expressions were significantly decreased when comparing co-cultures with WT monocytes to co-cultures with IL-15-deficient monocytes (Figures 5F and S5E), suggesting that the enhancement of their expression is dependent on IL-15 trans-presentation but not on OPN secretion. While BCL-2 expression was not impacted by the deficiency in OPN, flow cytometry Annexin V staining revealed a significant increase in the frequency and numbers of Annexin V$^+$ NK cells when comparing co-culture with OPN-KO or WT monocytes (Figure 5G). Complementation with recombinant OPN restored the level of apoptosis of NK cells in the OPN-KO condition (Figure 5G). Similar results of increased NK cell apoptosis were obtained in the IL-15-deficiency and single-culture conditions, although the difference in absolute numbers was not statistically significant for the IL-15-KO condition (Figure 5G). This can be explained by the lower total number of cells after 5 days of culture in the absence of IL-15 (Figure S5G). Because proliferation is not impacted by monocyte-derived IL-15 signaling (Figure S5H), the reduced final number of cells results from decreased survival.

To demonstrate the *in vivo* importance of the IL-15 trans-presentation to NK precursors from BM monocytes, we fed IL-15-KO mice with chow, MCD, and HFHG diets. When fed with MCD or HFHG diet, IL-15-deficient mice displayed no difference in BM NK precursor numbers (Figure S6A) and no upregulation of BCL-2, T-BET, and EOMES (Figure S6B). The frequency of circulating NK cells remained also unaffected (Figure S6C). On the other hand, hepatic NK cell numbers were significantly increased in NASH diets compared to chow-fed IL-15-KO mice (Figure S6C). Hence, IL-15 signaling is required for BM NK precursor accumulation and recruitment but not necessarily for liver NK cell expansion during DI-NASH.

These results highlight the fact that the need for liver NK cell expansion is paramount. *In situ* mechanisms probably take over and promote either the proliferation or survival of the "remaining" hepatic NK cells. In the absence of IL-15, we hypothesized that IL-2 can take over. IL-2 can induce NK cell proliferation *in vivo* when administered to patients[36] and can directly rescue human NK cells from apoptosis in a PI3K-dependent manner.[37] CD25 is upregulated at the surface of liver NK cells from mice fed with MCD diet, and this upregulation is conserved in the absence of IL-15 signaling, as it was also observed in IL-15-KO mice (Figure S6D).

Overall, this demonstrates that BM monocytes can promote NK cell maturation and survival through IL-15 trans-presentation and OPN secretion.

Monocyte-derived OPN promotes NK precursor survival, thus sustaining their recruitment to the liver

While OPN did not directly impact NK precursor survival (Figure S6E), it was proposed to prevent monocyte apoptosis.[38]

Figure 4. Diet-induced (DI) NASH promotes NK cell survival and maturation in the bone marrow (BM)

(A) Simplified diagram of adult BM NK cell development. rNKp, refined NK progenitor; iNK, immature NK; DP, double positive.

(B) Flow cytometric analyses, absolute numbers, and analyses of proliferation and survival of rNKp cells from chow-, MCD-, and HFHG-fed mice.

(C) Flow cytometric analyses and absolute numbers of iNK cells and NK precursors in chow, MCD, or HFHG diets.

(D) mRNA expression levels of maturation and survival factors on a FACS pool of iNK and CD27$^+$CD11b$^-$ NK cells.

(E) MFI of T-BET, EOMES, and BCL-2 in iNK and CD27$^+$CD11b$^-$ NK cells.

(F) FACS analyses of Thy1.2 and CXCR3 expression on BM NK precursors at steady state (left). MFI of CXCR3 on BM NK progenitors from mice fed with chow, MCD, and HFHG diets (right).

(G) mRNA expression of *S1pr5* on BM NK cells in the different diets.

Data are means ± SD of at least two independent experiments with at least two mice in each condition per experiment. *$p < 0.05$, **$p < 0.01$, ***$p < 0.001$, and ****$p < 0.0001$ by Mann-Whitney test.

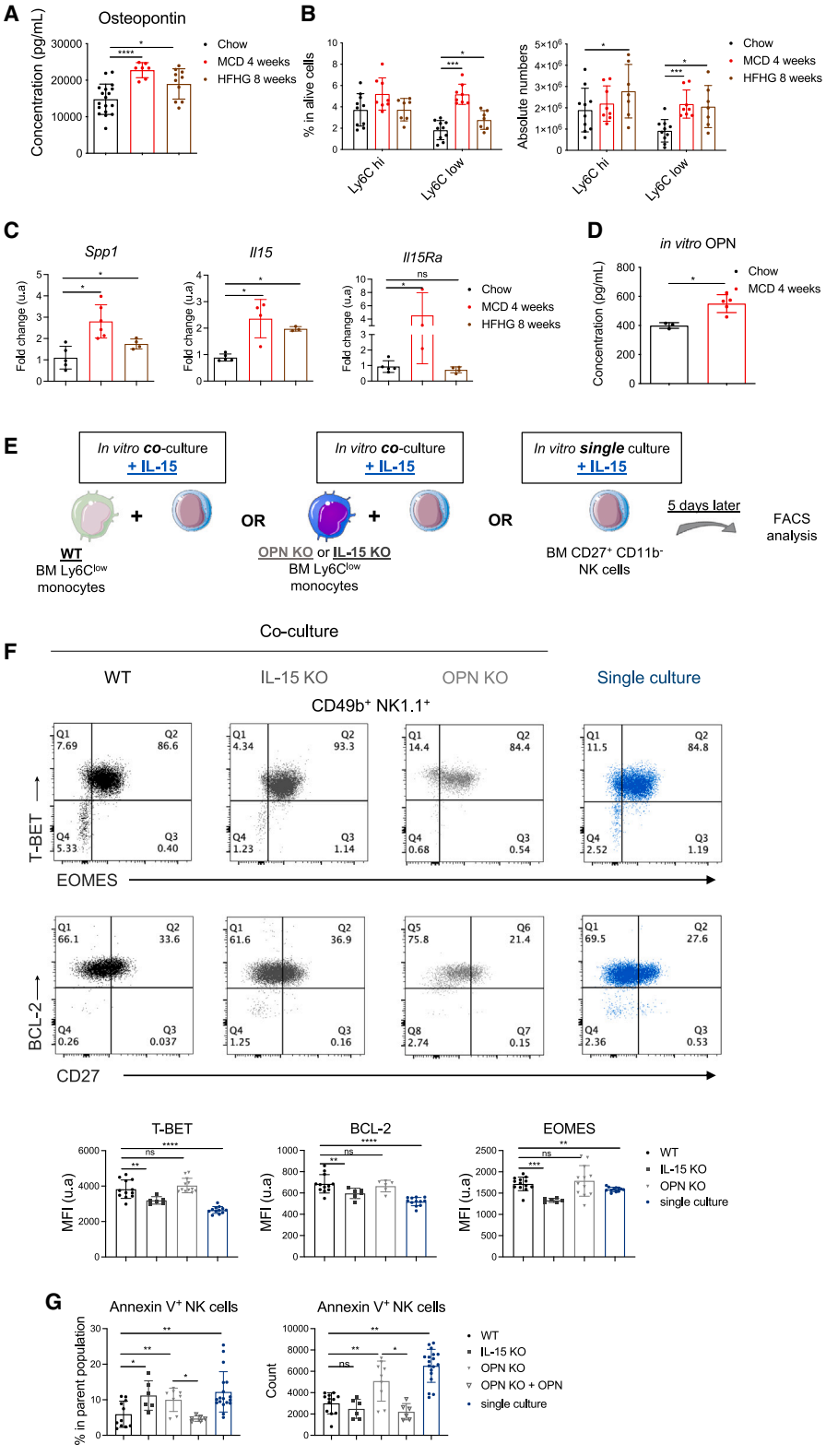

(legend on next page)

We cultured BM Ly6C^{low} monocytes without fetal calf serum and added OPN or macrophage colony-stimulating factor (M-CSF). After 3 days of incubation, the Annexin V level of fluorescence was significantly lower in OPN or M-CSF, suggesting decreased apoptosis (Figure 6A).

To determine the impact of OPN on BM monocyte accumulation and NK cell response in DI-NASH, we fed OPN-deficient mice with chow and NASH diets (Figure 6B). Absence of OPN led to a decrease in ALT and AST activity in MCD-diet-fed mice (Figure 6C). In the BM, Ly6C^{low} monocytes, CD27^{+}CD11b^{-}, and DP NK cells displayed no accumulation in MCD- and HFHG-fed OPN-KO mice compared to their chow-fed littermates (Figure 6D). Circulating and hepatic NK cells (Figure 6D) also showed a significant decrease in frequency and numbers when comparing WT and OPN-deficient mice. This suggests a reduced recruitment of NK cells to the liver in the absence of OPN. CXCR3 upregulation on recruited NK cells as well as upregulation of liver CXCL10 were both maintained in MCD-fed OPN-KO mice (Figure S6F), suggesting that this axis is independent of OPN. In accordance with the reduced recruitment of NK cells, liver Ly6C^{high} monocytes displayed significant upregulations of *Il10* and *Arg1* and decreased expressions of *Tnfa* and *Il1b* in MCD- and HFHG-fed, OPN-deficient mice compared to OPN-sufficient ones (Figure 6E). However, *Arg1* was also upregulated in chow-fed OPN-KO mice, suggesting that the absence of OPN, and not the absence of NK cell accumulation, is responsible for this enhanced expression in monocytes. Fibrogenesis-related genes, *Timp1* and *Col1a1*, were also upregulated in livers from MCD-fed OPN-KO mice compared to their WT counterparts (Figure S6G).

While steatosis was not affected, monocyte recruitment was reduced in OPN-deficient mice fed with MCD or HFHG diets compared to their WT counterparts (Figures 6F and S6H). OPN has been known to be a macrophage chemoattractant for decades.[39] Indeed, chronic exposure of WT mice to low doses of OPN resulted in haptic recruitment of Ly6C^{high} monocyte (Figure S6I). However, the NAS showed no significant difference between WT and OPN-KO mice (Figures 6C and S6J).

We conclude that OPN deficiency results in the abrogation of DI-enhanced BM monocyte survival, leading to an absence of NK precursor accumulation and subsequent decreased NK cell recruitment to the liver. Altogether, our results unveil a role for BM-monocyte-derived OPN in regulating NK cell immune response during DI-NASH.

Endotoxemia participates in liver NK cell recruitment by enhancing BM monocyte production of IL-15/IL-15Rα and OPN

Patients suffering from NASH usually display gut dysbiosis and impaired intestinal barrier, which leads to an increased amount of endotoxins entering the liver through the portal vein.[40] Using the intestinal permeability assay, we showed significantly higher quantities of circulating dextran in MCD-fed mice compared to chow-fed mice, indicating an increased gut permeability (Figure 7A). Toll-like receptor 2 (TLR2) and TLR4, both involved in gram-negative-bacteria-derived PAMP recognition,[41] were upregulated in the liver of MCD-diet-fed mice (Figure 7B).

A common model to study endotoxemia in mice consists in intraperitoneally (i.p.) injecting lipopolysaccharide (LPS). LPS binds to TLR4 and can signal through Myd88 adaptor protein.[42] Mice submitted to one single LPS injection were analyzed 24 h later (Figure S7A). The elevated AST levels revealed inflammation-related injury, while hepatic inflammation was not especially noted (no change in ALT activity) (Figure S7B).

In LPS-injected mice, the frequency of circulating and liver NK cells was 3-fold higher than in the MCD-diet-fed mice (Figure S7C). In the BM, the frequency of NK precursors (DP stage) was increased in LPS-injected mice, which could indicate an accelerated maturation process (Figure S7D). BM cellularity is reduced in case of LPS injection, explaining the reduction of NK progenitor number despite the increase of their ferquency (Figure S7D). This drop most likely results from endotoxemia-driven emergency myelopoiesis characterized by mobilization of neutrophils and expansion of the myeloid compartment at the expense of leukocytes.[43,44] To determine whether LPS signaling is necessary for NK cell recruitment in DI-NASH, we fed Myd88-KO mice with chow and MCD diets. In the absence of PAMP signaling, *Tlr2* and *Tlr4* expressions were significantly decreased (Figure 7B), while ALT and AST activities were not impacted (Figure 7C). BM CD27^{+}CD11b^{-} and DP NK cell numbers showed no augmentation in MCD-fed, Myd88-deficient mice, suggesting that PAMPs play a role in NASH-induced NK precursor accumulation (Figure 7D). In the absence of Myd88, the increase in BM OPN concentration was lost (Figure 7E). BM Ly6C^{low} monocyte numbers were decreased (Figure 7F), and the MCD-induced upregulation of *IL15*, *IL15Ra*, and *Spp1* was abrogated (Figure 7G). Hepatic NK cells were significantly decreased in frequency and numbers when compared to MCD-fed WT mice (Figure 7H).

Figure 5. BM Ly6C^{low} monocytes positively regulate NK cell maturation and survival during DI-NASH via IL-15 trans-presentation and OPN secretion

(A–C) Titration of OPN in BM supernatants (A), percentage and absolute numbers of BM Ly6C^{high} and Ly6C^{low} monocytes (B), and mRNA expression levels of *Il15*, *IL15Ra*, and *Spp1* in FACS BM Ly6C^{low} monocytes (C) from chow-, MCD-, and HFHG-fed mice.

(D) Supernatant OPN concentration from FACS BM Ly6C^{low} monocytes cultured for 18 h.

(E) Experimental design of the co-cultures.

(F) Flow cytometric analyses and MFI of T-BET, BCL-2, and EOMES expressions from CD27^{+}CD11b^{-} cell/Ly6C^{low} monocyte co-cultures versus single culture of CD27^{+}CD11b^{-} NK cells.

(G) Frequency and numbers of Annexin V^{+} NK cells. Recombinant mouse OPN was added in one condition of co-culture with OPN-KO BM Ly6C^{low} monocytes.

Data are means ± SD of at least two independent experiments with at least three replicates in each condition per experiment. *$p < 0.05$, **$p < 0.01$, ***$p < 0.001$, and ****$p < 0.0001$ by Mann-Whitney test.

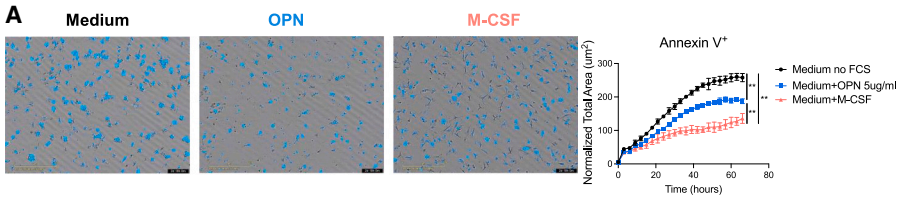

C

	WT			OPN KO		
	Chow	MCD	HFHG	Chow	MCD	HFHG
ALT	10,33 ± 8,23	786,05 ± 389,76	33,44 ± 24,48	9,5 ± 9,29	23 ± 20,24	29 ± 20,01
AST	165,9 ± 85,75	655,16 ± 247,42	168,11 ± 119,28	217,75 ± 121,04	264,6 ± 35,91	92,25 ± 42,29
NAS Score	-	2,69 ± 0,49	1,94 ± 0,56	-	2,28 ± 0,14	1,96 ± 0,77

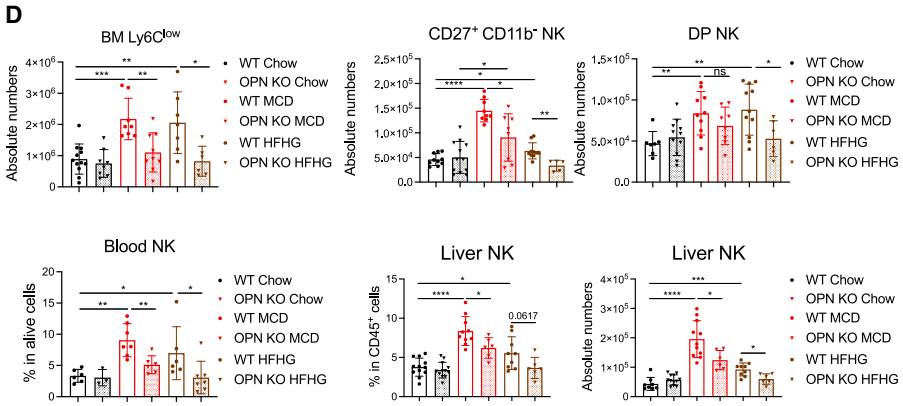

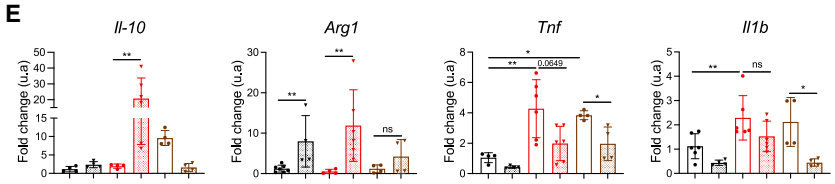

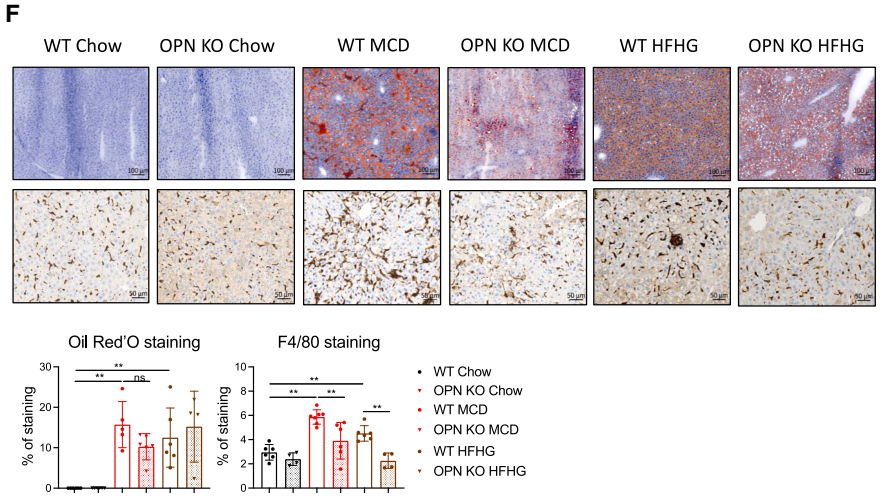

(legend on next page)

Altogether, our data reveal that Myd88 signaling is responsible for the enhancement of BM monocyte production of IL-15/IL-15Rα and OPN in DI-NASH leading to NK precursor accumulation (Figure 7G).

Overall, our work links the gut, liver, and BM in a triad for an increased NK cell response during DI-NASH.

DISCUSSION

NASH is a multifactorial pathogenesis in which hepatocyte lipotoxicity and immune-mediated inflammation are crucial in driving the disease progression. Inflammation could impact immune cell development,[45] and our results point out that DI-NASH specifically promotes central NK cell-poiesis. We demonstrate that the recruitment of NK cells is sustained by enhanced BM NK cell production via the expansion of proliferating progenitors and an accumulation of precursors. The accumulation of BM $CD27^{+}CD11b^{-}$ and DP NK cell subsets results from the upregulation of IL-15-dependent survival and maturation gene programs (*Tbx21*, *Prdm1, Eomes*, *Klf2*, etc.).

Dysregulations along the gut-liver axis are associated with NASH partially contributing to liver injury and inflammation. The systemic increase of PAMPs related to intestinal permeability are the most probable factors disrupting the gut-liver axis.[46,47] We showed that endotoxemia participates to the hepatic NK cell recruitment. The latter was not fully abrogated in Myd88-KO mice, suggesting that endotoxemia is not the only mechanism at play. Lipotoxicity might also be involved in the recruitment of hepatic NK cells.[48,49]

OPN is a biomarker for liver diseases including NASH, cirrhosis, and HCC in humans.[50,51] OPN is one of the major proteins secreted in the BM under DI inflammation compared to levels of production of typical adipokines such as leptin. BM monocytes, which produce both OPN and the IL-15/IL-15Rα complex, are increased in numbers and upregulate *IL15*, *IL15Ra*, and *Spp1* transcripts in DI-NASH-fed mice. BM $Ly6C^{low}$ monocytes can directly enhance NK precursor maturation and survival through IL-15/IL-15Rα trans-presentation. The secretion of OPN by BM monocytes does not directly impact NK precursors but rather monocytes themselves, with an increased survival. In OPN-deficient mice fed with NASH-inducing diets, the accumulation of monocytes in the BM was abrogated. We propose that this increased monocyte survival enhances the numbers of potential IL-15 trans-presenting cells. As OPN-KO mice lack both iOPN and sOPN isoforms, the defect in NASH-driven monocyte accumulation could be partly due to the absence of iOPN. Nonetheless, our competitive reconstitution experiments demonstrated that the survival and accumulation of NK precursors and hepatic NK cells are mostly driven by external NASH-favoring factors.

The crosstalk between monocytes and NK cells was proposed in peripheral organs with a monocyte-mediated mechanism that sustains terminal differentiation of splenic murine NK cells in an IL-15/IL-15Rα manner.[52] Our results indicate that BM monocytes participate to shape the NK cell functional maturation during DI-NASH.

The role of hepatic NK cells on liver inflammation is still controversial. Numerous studies used mouse models that delete NK cells from the first embryonic stage, somehow impairing normal liver organogenesis and blurring the conclusion on their specific functions. In our diet context, using temporary or complete depletion of NK cells, we confirmed that hepatic NK cells restrict $Ly6C^{high}$ monocyte recruitment and postulate that this inhibition possibly takes place via ligand competition for CCL2. Indeed, liver NK cells express CCR2, albeit to a lesser extent than monocytes. The absence of NK cells leads to an increased availability of CCL2, which may explain the observed rise in monocyte recruitment. We also observed an upregulation of *Tnfsf10* (coding for TRAIL) in hepatic NK cells from MCD- or HFHG-fed mice as well as a decreased $Ly6C^{high}$ monocyte death in the absence of NK cells. These results suggest that liver NK cells may eliminate recruited monocytes in a TRAIL-dependent manner. We also validated that hepatic NK cells the direct recruited monocyte profile toward an M1 pro-inflammatory signature.[17]

Other studies have described similar NK cell role on $Ly6C^{low}$ infiltrating monocytes.[4,5] The upregulation of fibrosis-related genes in liver of MCD-fed, NK-cell-deficient mice compared to their NK-cell-sufficient counterparts underlines the anti-fibrotic role of recruited NK cells. The implication of the increased number of activated NKs in the liver on the slowing down of the fibrogenesis program is also reinforced by the observed tendency to decrease the fibrogenic signature in OPN-deficient mice containing less NK cells. NK cells are prone to kill activated HSCs.[16] Our data suggest that NK cells have multiple roles during DI-NASH, limiting its progression toward fibrosis and restricting the recruitment of monocytes while polarizing them toward a pro-inflammatory phenotype.

Our results highlight a mechanistic process by which inflammation (provided by lipotoxicity, immune inflammatory cells, and endotoxemia) affects NK cell development and functional maturation. IL-15 and OPN are the two main factors at play in this regulation at early stages of DI-NASH. Both NASH diets

Figure 6. Monocyte-derived osteopontin directly promotes NK precursor survival, thus sustaining their recruitment to the liver

(A) Analysis of apoptosis of BM $Ly6C^{low}$ monocytes cultured without FCS and with or without OPN or M-CSF. MFI of each well at each time point was normalized by cell number.

(B) Experimental model scheme.

(C) Individual scores and NAS.

(D) Absolute numbers of BM $Ly6C^{low}$ monocytes and $CD27^{+}CD11b^{-}$ and DP NK cells, frequency of blood NK cells, and percentage and numbers of liver NK cells in chow-, MCD-, or HFHG-fed WT and OPN-KO mice.

(E) Representative images and quantitative analyses of oil red O (top) and F4/80 (bottom) staining of livers from OPN-sufficient and -deficient mice fed with chow, MCD, or HFHG diets.

(F) mRNA expression levels of genes in FACS liver $Ly6C^{high}$ monocytes from chow- and MCD-fed WT and OPN-KO mice.

Data are means ± SD of at least two independent experiments with at least two mice in each condition per experiment. $^{*}p < 0.05$, $^{**}p < 0.01$, $^{***}p < 0.001$, and $^{****}p < 0.0001$ by Mann-Whitney test.

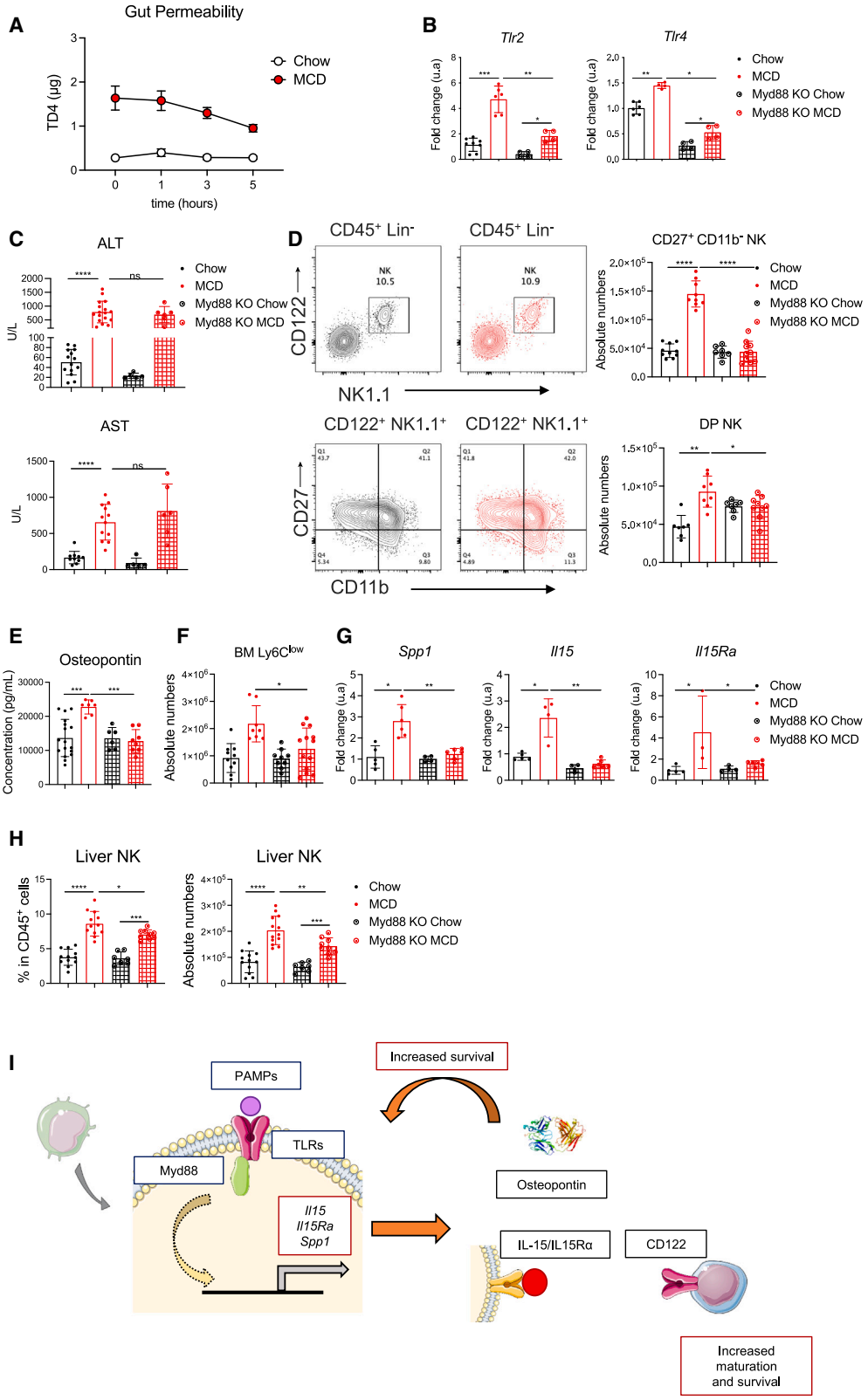

(legend on next page)

exhibit this cellular crosstalk, strengthening the importance of maintaining NK cell accumulation to limit the progression of NASH.

In conclusion, we present a paradigm for how BM monocytes can shape the NK progenitor/precursor pool in the first stages of the pathology to participate to the slowdown of the disease progression. Future research focused on patients with NASH would be required to know whether these mechanisms translate to humans. Having a better understanding of the events controlling NK cell response in NAFLD will help with setting up new therapeutic strategies.

Limitations of the study

It will be important to translate our findings to the human pathology. Confirmation of an increased recruitment of NK cells may be done using blood samples and liver biopsies from patients with NASH. Analyses of circulating human NK cells with an enrichment in CD56^{bright} NK cells would also help corroborate an enhanced NK cell-poiesis. It would be of significance to study later stages of the disease, notably the transition toward a fibrotic state of the liver, to clarify the role of NK cells in that context.

STAR★METHODS

Detailed methods are provided in the online version of this paper and include the following:

- KEY RESOURCES TABLE
- RESOURCE AVAILABILITY
  - Lead contact
  - Materials availability
  - Data and code availability
- EXPERIMENTAL MODEL AND STUDY PARTICIPANT DETAILS
  - *In vivo* animal studies
- METHOD DETAILS
  - Flow cytometry and cell sorting
  - Tissue dissociation
  - Co-culture assay
  - Cell culture and apoptosis assays
  - Cell proliferation assay
  - NK cell depletion
  - Quantification of proteins
  - RNA extraction and RT-qPCR
  - Biochemical analysis
  - Histology
  - Oral glucose tolerance test (OGTT) and Insuline tolerance test (ITT)
  - Intestinal paracellular permeability test
  - BM reconstitution
- QUANTIFICATION AND STATISTICAL ANALYSIS
  - Bioinformatics
  - Statistical analysis

SUPPLEMENTAL INFORMATION

Supplemental information can be found online at https://doi.org/10.1016/j.celrep.2024.113676.

ACKNOWLEDGMENTS

We are grateful to D. Hardy, M. Tichit, and J. Bedel from the Histopathology Core Facility of the Institut Pasteur for technical support and histological sections of livers. We acknowledge the Cytometry and Biomarkers Unit of Technology and Service (CB UtechS) at the Institut Pasteur for support and specifically thank S. Megharba, L. Barrio Cano, and E. Karkeni for their help. We thank the staff of the Animal Facility of the Institut Pasteur for mouse care. We thank L. Debarbieux for Myd88-deficient mice, P. Bousso for IFNγ-deficient mice, and P. Vieira for IL-15-KO mice. We thank G. Eberl and E. Lecuyer for providing the technical assay to measure gut permeability. We are grateful to B. Staels and D. Dombrowicz for their advice on the HFD used and for providing insulin tolerance test protocols. We are grateful to J.-P. Couty for sharing his expertise on liver inflammation. This work has been supported by Institut Pasteur, Université Paris Cité, Institut National de la Santé et de la Recherche Médicale (INSERM), and by grants from INSERM by the French government (National Research Agency, ANR), ANR project NASHILCCD8 (#18-CE15-0024-01). E.B. is funded by La Ligue Contre Le Cancer (ref: IP/SC-17531).

AUTHOR CONTRIBUTIONS

E.B. designed the studies, performed most experiments, analyzed data, constructed figures, and wrote the manuscript. T.P. initiated the project, set up diet models, designed studies, performed experiments, and analyzed data. S.M. gave guidance on the design and performed experiments. H.B. assisted E.B. during experiments. M.-P.M. performed RNA extraction and quantitative real-time PCR experiments. E.M. bred and provided the OPN-deficient mice. A.C. contributed to the discussions for the manuscript. R.G. directed the research, designed the studies, analyzed data, and wrote the manuscript.

DECLARATION OF INTERESTS

The authors declare no competing interests.

Figure 7. Endotoxemia participates to liver NK cell recruitment by enhancing BM monocyte production of IL-15/IL-15Rα and OPN

(A) Gut permeability in chow- and MCD-fed mice.
(B) Relative mRNA expression of *Tlr2* and *Tlr4* in liver tissue from WT and Myd88-KO mice.
(C) Individual scores and NAS.
(D) Flow cytometric analyses and percentage and numbers of NK precursors in WT and Myd88-KO mice.
(E) Titration of OPN in BM supernatants.
(F) Numbers of BM Ly6C^{low} monocytes in the different conditions.
(G) mRNA expression levels of *Il15*, *IL15Ra*, and *Spp1* in FACS Myd88-sufficient or -deficient BM Ly6C^{low} monocytes.
(H) Frequency and numbers of livers NK cells in WT and Myd88-KO mice.
(I) Scheme of the proposed mechanism.
Data are means ± SD of at least two independent experiments with at least two mice in each condition per experiment. *$p < 0.05$, **$p < 0.01$, ***$p < 0.001$, and ****$p < 0.0001$ by Mann-Whitney test.

Received: July 14, 2023
Revised: November 22, 2023
Accepted: January 2, 2024

REFERENCES

1. Estes, C., Razavi, H., Loomba, R., Younossi, Z., and Sanyal, A.J. (2018). Modeling the epidemic of nonalcoholic fatty liver disease demonstrates an exponential increase in burden of disease. Hepatol. Baltim. Md *67*, 123–133.
2. Van Herck, M.A., Weyler, J., Kwanten, W.J., Dirinck, E.L., De Winter, B.Y., Francque, S.M., and Vonghia, L. (2019). The Differential Roles of T Cells in Non-alcoholic Fatty Liver Disease and Obesity. Front. Immunol. *10*, 82.
3. Wolf, M.J., Adili, A., Piotrowitz, K., Abdullah, Z., Boege, Y., Stemmer, K., Ringelhan, M., Simonavicius, N., Egger, M., Wohlleber, D., et al. (2014). Metabolic activation of intrahepatic CD8+ T cells and NKT cells causes nonalcoholic steatohepatitis and liver cancer via cross-talk with hepatocytes. Cancer Cell *26*, 549–564.
4. Fan, Y., Zhang, W., Wei, H., Sun, R., Tian, Z., and Chen, Y. (2020). Hepatic NK cells attenuate fibrosis progression of non-alcoholic steatohepatitis in dependent of CXCL10-mediated recruitment. Liver Int. *40*, 598–608.
5. Tosello-Trampont, A.-C., Krueger, P., Narayanan, S., Landes, S.G., Leitinger, N., and Hahn, Y.S. (2016). NKp46(+) natural killer cells attenuate metabolism-induced hepatic fibrosis by regulating macrophage activation in mice. Hepatol. Baltim. Md *63*, 799–812.
6. Wang, F., Zhang, X., Liu, W., Zhou, Y., Wei, W., Liu, D., Wong, C.C., Sung, J.J.Y., and Yu, J. (2022). Activated Natural Killer Cell Promotes Nonalcoholic Steatohepatitis Through Mediating JAK/STAT Pathway. Cell. Mol. Gastroenterol. Hepatol. *13*, 257–274.
7. Luci, C., Vieira, E., Perchet, T., Gual, P., and Golub, R. (2019). Natural Killer Cells and Type 1 Innate Lymphoid Cells Are New Actors in Non-alcoholic Fatty Liver Disease. Front. Immunol. *10*, 1192.
8. Luci, C., Bourinet, M., Leclère, P.S., Anty, R., and Gual, P. (2020). Chronic Inflammation in Non-Alcoholic Steatohepatitis: Molecular Mechanisms and Therapeutic Strategies. Front. Endocrinol. *11*, 597648.
9. Cepero-Donates, Y., Lacraz, G., Ghobadi, F., Rakotoarivelo, V., Orkhis, S., Mayhue, M., Chen, Y.-G., Rola-Pleszczynski, M., Menendez, A., Ilangumaran, S., and Ramanathan, S. (2016). Interleukin-15-mediated inflammation promotes non-alcoholic fatty liver disease. Cytokine *82*, 102–111.
10. Artis, D., and Spits, H. (2015). The biology of innate lymphoid cells. Nature *517*, 293–301.
11. Chen, Y., Wang, X., Hao, X., Li, B., Tao, W., Zhu, S., Qu, K., Wei, H., Sun, R., Peng, H., and Tian, Z. (2022). Ly49E separates liver ILC1s into embryo-derived and postnatal subsets with different functions. J. Exp. Med. *219*, e20211805.
12. Topham, N.J., and Hewitt, E.W. (2009). Natural killer cell cytotoxicity: how do they pull the trigger? Immunology *128*, 7–15.
13. Bai, L., Vienne, M., Tang, L., Kerdiles, Y., Etiennot, M., Escalière, B., Galluso, J., Wei, H., Sun, R., Vivier, E., et al. (2021). Liver type 1 innate lymphoid cells develop locally via an interferon-γ-dependent loop. Science *371*, eaba4177.
14. Friedrich, C., Taggenbrock, R.L.R.E., Doucet-Ladevèze, R., Golda, G., Moenius, R., Arampatzi, P., Kragten, N.A.M., Kreymborg, K., Gomez de Agüero, M., Kastenmüller, W., et al. (2021). Effector differentiation downstream of lineage commitment in ILC1s is driven by Hobit across tissues. Nat. Immunol. *22*, 1256–1267.
15. Radaeva, S., Sun, R., Jaruga, B., Nguyen, V.T., Tian, Z., and Gao, B. (2006). Natural killer cells ameliorate liver fibrosis by killing activated stellate cells in NKG2D-dependent and tumor necrosis factor-related apoptosis-inducing ligand-dependent manners. Gastroenterology *130*, 435–452.
16. Melhem, A., Muhanna, N., Bishara, A., Alvarez, C.E., Ilan, Y., Bishara, T., Horani, A., Nassar, M., Friedman, S.L., and Safadi, R. (2006). Anti-fibrotic activity of NK cells in experimental liver injury through killing of activated HSC. J. Hepatol. *45*, 60–71.
17. Remmerie, A., Martens, L., Thoné, T., Castoldi, A., Seurinck, R., Pavie, B., Roels, J., Vanneste, B., De Prijck, S., Vanhockerhout, M., et al. (2020). Osteopontin Expression Identifies a Subset of Recruited Macrophages Distinct from Kupffer Cells in the Fatty Liver. Immunity *53*, 641–657.e14.
18. Krenkel, O., Hundertmark, J., Abdallah, A.T., Kohlhepp, M., Puengel, T., Roth, T., Branco, D.P.P., Mossanen, J.C., Luedde, T., Trautwein, C., et al. (2020). Myeloid cells in liver and bone marrow acquire a functionally distinct inflammatory phenotype during obesity-related steatohepatitis. Gut *69*, 551–563.
19. Seidman, J.S., Troutman, T.D., Sakai, M., Gola, A., Spann, N.J., Bennett, H., Bruni, C.M., Ouyang, Z., Li, R.Z., Sun, X., et al. (2020). Niche-Specific Reprogramming of Epigenetic Landscapes Drives Myeloid Cell Diversity in Nonalcoholic Steatohepatitis. Immunity *52*, 1057–1074.e7.
20. Krenkel, O., Puengel, T., Govaere, O., Abdallah, A.T., Mossanen, J.C., Kohlhepp, M., Liepelt, A., Lefebvre, E., Luedde, T., Hellerbrand, C., et al. (2018). Therapeutic inhibition of inflammatory monocyte recruitment reduces steatohepatitis and liver fibrosis. Hepatol. Baltim. Md *67*, 1270–1283.
21. Hou, X., Yin, S., Ren, R., Liu, S., Yong, L., Liu, Y., Li, Y., Zheng, M.-H., Kunos, G., Gao, B., and Wang, H. (2021). Myeloid-Cell-Specific IL-6 Signaling Promotes MicroRNA-223-Enriched Exosome Production to Attenuate NAFLD-Associated Fibrosis. Hepatol. Baltim. Md *74*, 116–132.
22. Puengel, T., Lefere, S., Hundertmark, J., Kohlhepp, M., Penners, C., Van de Velde, F., Lapauw, B., Hoorens, A., Devisscher, L., Geerts, A., et al. (2022). Combined Therapy with a CCR2/CCR5 Antagonist and FGF21 Analogue Synergizes in Ameliorating Steatohepatitis and Fibrosis. Int. J. Mol. Sci. *23*, 6696.
23. Groom, J.R., and Luster, A.D. (2011). CXCR3 ligands: redundant, collaborative and antagonistic functions. Immunol. Cell Biol. *89*, 207–215.
24. Brownell, J., Bruckner, J., Wagoner, J., Thomas, E., Loo, Y.-M., Gale, M., Liang, T.J., and Polyak, S.J. (2014). Direct, interferon-independent activation of the CXCL10 promoter by NF-κB and interferon regulatory factor 3 during hepatitis C virus infection. J. Virol. *88*, 1582–1590.
25. Qiao, J.T., Cui, C., Qing, L., Wang, L.S., He, T.Y., Yan, F., Liu, F.Q., Shen, Y.H., Hou, X.G., and Chen, L. (2018). Activation of the STING-IRF3 pathway promotes hepatocyte inflammation, apoptosis and induces metabolic disorders in nonalcoholic fatty liver disease. Metabolism *81*, 13–24.
26. Chiossone, L., Chaix, J., Fuseri, N., Roth, C., Vivier, E., and Walzer, T. (2009). Maturation of mouse NK cells is a 4-stage developmental program. Blood *113*, 5488–5496.
27. Jenne, C.N., Enders, A., Rivera, R., Watson, S.R., Bankovich, A.J., Pereira, J.P., Xu, Y., Roots, C.M., Beilke, J.N., Banerjee, A., et al. (2009). T-bet-dependent S1P5 expression in NK cells promotes egress from lymph nodes and bone marrow. J. Exp. Med. *206*, 2469–2481.
28. Constantinides, M.G., Gudjonson, H., McDonald, B.D., Ishizuka, I.E., Verhoef, P.A., Dinner, A.R., and Bendelac, A. (2015). PLZF expression maps the early stages of ILC1 lineage development. Proc. Natl. Acad. Sci. USA *112*, 5123–5128.
29. Klose, C.S.N., Flach, M., Möhle, L., Rogell, L., Hoyler, T., Ebert, K., Fabiunke, C., Pfeifer, D., Sexl, V., Fonseca-Pereira, D., et al. (2014). Differentiation of type 1 ILCs from a common progenitor to all helper-like innate lymphoid cell lineages. Cell *157*, 340–356.
30. Kallies, A., Carotta, S., Huntington, N.D., Bernard, N.J., Tarlinton, D.M., Smyth, M.J., and Nutt, S.L. (2011). A role for Blimp1 in the transcriptional network controlling natural killer cell maturation. Blood *117*, 1869–1879.
31. Rabacal, W., Pabbisetty, S.K., Hoek, K.L., Cendron, D., Guo, Y., Maseda, D., and Sebzda, E. (2016). Transcription factor KLF2 regulates homeostatic NK cell proliferation and survival. Proc. Natl. Acad. Sci. USA *113*, 5370–5375.

32. Johnston, J.A., Bacon, C.M., Finbloom, D.S., Rees, R.C., Kaplan, D., Shibuya, K., Ortaldo, J.R., Gupta, S., Chen, Y.Q., and Giri, J.D. (1995). Tyrosine phosphorylation and activation of STAT5, STAT3, and Janus kinases by interleukins 2 and 15. Proc. Natl. Acad. Sci. USA *92*, 8705–8709.

33. Nilsson, S.K., Johnston, H.M., Whitty, G.A., Williams, B., Webb, R.J., Denhardt, D.T., Bertoncello, I., Bendall, L.J., Simmons, P.J., and Haylock, D.N. (2005). Osteopontin, a key component of the hematopoietic stem cell niche and regulator of primitive hematopoietic progenitor cells. Blood *106*, 1232–1239.

34. Maeda, Y., Yonemochi, Y., Nakajyo, Y., Hidaka, H., Ikeda, T., and Ando, Y. (2017). CXCL12 and osteopontin from bone marrow-derived mesenchymal stromal cells improve muscle regeneration. Sci. Rep. *7*, 3305.

35. Nagoshi, S. (2014). Osteopontin: Versatile modulator of liver diseases. Hepatol. Res. *44*, 22–30.

36. Miller, J.S., Soignier, Y., Panoskaltsis-Mortari, A., McNearney, S.A., Yun, G.H., Fautsch, S.K., McKenna, D., Le, C., Defor, T.E., Burns, L.J., et al. (2005). Successful adoptive transfer and in vivo expansion of human haploidentical NK cells in patients with cancer. Blood *105*, 3051–3057.

37. Taguchi, Y., Kondo, T., Watanabe, M., Miyaji, M., Umehara, H., Kozutsumi, Y., and Okazaki, T. (2004). Interleukin-2-induced survival of natural killer (NK) cells involving phosphatidylinositol-3 kinase-dependent reduction of ceramide through acid sphingomyelinase, sphingomyelin synthase, and glucosylceramide synthase. Blood *104*, 3285–3293.

38. Burdo, T.H., Wood, M.R., and Fox, H.S. (2007). Osteopontin prevents monocyte recirculation and apoptosis. J. Leukoc. Biol. *81*, 1504–1511.

39. Wüthrich, R.P., Fan, X., Ritthaler, T., Sibalic, V., Yu, D.J., Loffing, J., and Kaissling, B. (1998). Enhanced osteopontin expression and macrophage infiltration in MRL-Fas(lpr) mice with lupus nephritis. Autoimmunity *28*, 139–150.

40. Henao-Mejia, J., Elinav, E., Jin, C., Hao, L., Mehal, W.Z., Strowig, T., Thaiss, C.A., Kau, A.L., Eisenbarth, S.C., Jurczak, M.J., et al. (2012). Inflammasome-mediated dysbiosis regulates progression of NAFLD and obesity. Nature *482*, 179–185.

41. Mukherjee, S., Karmakar, S., and Babu, S.P.S. (2016). TLR2 and TLR4 mediated host immune responses in major infectious diseases: a review. Braz. J. Infect. Dis. *20*, 193–204.

42. Pålsson-McDermott, E.M., and O'Neill, L.A.J. (2004). Signal transduction by the lipopolysaccharide receptor, Toll-like receptor-4. Immunology *113*, 153–162.

43. Boettcher, S., Ziegler, P., Schmid, M.A., Takizawa, H., van Rooijen, N., Kopf, M., Heikenwalder, M., and Manz, M.G. (2012). Cutting edge: LPS-induced emergency myelopoiesis depends on TLR4-expressing nonhematopoietic cells. J. Immunol. Md 1950 *188*, 5824–5828.

44. Skirecki, T., Kawiak, J., Machaj, E., Pojda, Z., Wasilewska, D., Czubak, J., and Hoser, G. (2015). Early severe impairment of hematopoietic stem and progenitor cells from the bone marrow caused by CLP sepsis and endotoxemia in a humanized mice model. Stem Cell Res. Ther. *6*, 142.

45. Bourayou, E., and Golub, R. (2022). Inflammatory-driven NK cell maturation and its impact on pathology. Front. Immunol. *13*, 1061959.

46. Luther, J., Garber, J.J., Khalili, H., Dave, M., Bale, S.S., Jindal, R., Motola, D.L., Luther, S., Bohr, S., Jeoung, S.W., et al. (2015). Hepatic Injury in Nonalcoholic Steatohepatitis Contributes to Altered Intestinal Permeability. Cell. Mol. Gastroenterol. Hepatol. *1*, 222–232.

47. Schubert, K., Olde Damink, S.W.M., von Bergen, M., and Schaap, F.G. (2017). Interactions between bile salts, gut microbiota, and hepatic innate immunity. Immunol. Rev. *279*, 23–35.

48. Zámbó, V., Simon-Szabó, L., Szelényi, P., Kereszturi, E., Bánhegyi, G., and Csala, M. (2013). Lipotoxicity in the liver. World J. Hepatol. *5*, 550–557.

49. Engin, A.B. (2017). What Is Lipotoxicity? Adv. Exp. Med. Biol. *960*, 197–220.

50. Leung, T.-M., Wang, X., Kitamura, N., Fiel, M.I., and Nieto, N. (2013). Osteopontin delays resolution of liver fibrosis. Lab. Invest. *93*, 1082–1089.

51. Sun, T., Tang, Y., Sun, D., Bu, Q., and Li, P. (2018). Osteopontin versus alpha-fetoprotein as a diagnostic marker for hepatocellular carcinoma: a meta-analysis. OncoTargets Ther. *11*, 8925–8935.

52. Soderquest, K., Powell, N., Luci, C., van Rooijen, N., Hidalgo, A., Geissmann, F., Walzer, T., Lord, G.M., and Martín-Fontecha, A. (2011). Monocytes control natural killer cell differentiation to effector phenotypes. Blood *117*, 4511–4518.

STAR★METHODS

KEY RESOURCES TABLE

REAGENT or RESOURCE	SOURCE	IDENTIFIER
Antibodies		
Ly76 (TER119)	Sony	Cat# 1181020; RRID:AB_3083430
Gr-1 (RB6-8C5)	Sony	Cat# 1142020;RRID:AB_3083431
CD3e (145-2C11)	BD Biosciences	Cat# 563565; RRID:AB_2738278
CD19 (MB19-1)	BD Biosciences	Cat# 553784; RRID:AB_395048
NK1.1 (PK136)	BD Biosciences	Cat# 564143; RRID:AB_2738617
IL-7Ra (A7R34)	Sony	Cat# 1275070; RRID:AB_3083432
CD8a (53-6.7)	Sony	Cat# 1103520;RRID:AB_3083433
CD4 (RM4-5)	Sony	Cat#1102540;RRID:AB_3083434
Thy1.2 (53-2.1)	BD Biosciences	Cat# 563008; RRID:AB_2665477
NKp46 (29A1.4)	BD Biosciences	Cat# 560756; RRID:AB_1727465
IFNg (XMG1.2)	BD Biosciences	Cat# 563773; RRID:AB_2738419
CD45.2 (104)	BD Biosciences	Cat# 563686; RRID:AB_2738375
CD49a (HMa1)	BD Biosciences	Cat# 564863; RRID:AB_2738987
CD49b (DX5)	BD Biosciences	Cat# 740133; RRID:AB_2739890
T-BET (4B10)	Sony	Cat# 3824020; RRID:AB_3083437
EOMES (Dan11mag)	eBioscience	Cat# 48-4875-82; RRID:AB_2574062
BCL-2 (BCL/10C4)	Sony	Cat# 3767520; RRID:AB_3083435
TNFa (MP6-XT22)	Sony	Cat# 3131620;RRID:AB_3083436
CD11b (M1/70)	BD Biosciences	Cat# 557960; RRID:AB_396960
CD11c (HL3)	BD Biosciences	Cat# 563735; RRID:AB_2738394
Granzyme B (GB12)	Invitrogen	Cat# MHGB04; RRID:AB_1500191
F4/80 (BM8)	Sony	Cat# 1215570; RRID:AB_3083438
MHCII (M5/114.15.2)	BD Biosciences	Cat# 563414; RRID:AB_2738191
CD226 (10E5)	BD Biosciences	Cat#565663; RRID:AB_2916365
CD94 (18d3)	BD Biosciences	Cat# 740951; RRID:AB_2740576
NKG2A (16A11)	BD Biosciences	Cat# 569527; RRID:AB_3083440
NKG2D (CX5)	BD Biosciences	Cat# 563694; RRID:AB_2722498
Ly6C (HK1.4)	Sony	Cat# 1240070; RRID:AB_3083349
Ly6G (1A8)	BD Biosciences	Cat# 551461; RRID:AB_394208
CD45 (30-F11)	BD Biosciences	Cat# 557659; RRID:AB_396774
CD122 (TM-b1)	BD Biosciences	Cat#553362; RRID:AB_394809
CD183 (CXCR3-173)	BD Biosciences	Cat#562266; RRID:AB_11153500
CD27 (LG.3A10)	Sony	Cat# 1221130
CD51 (RMV-7)	eBioscience	Cat#12-0512-82;RRID:AB_465704
CD44 (IM-7)	BD Biosciences	Cat#560569; RRID:AB_1727484
Ki67 (B56)	BD Biosciences	Cat#561165; RRID:AB_10611866
F4/80 (BM8)	eBioscience	Cat# 14-4801-82; RRID:AB_467558
CD25	BD Biosciences	Cat#553866; RRID:AB_395101
anti-asialo GM1 antibody	Invitrogen	Cat# 16-6507-39; RRID:AB_10718540
Chemicals, peptides, and recombinant proteins		
5-BrdU	R&D systems	Cat# 5015
Recombinant Mouse Osteopontin	R&D systems	Cat# 441-OP-050/CF
Recombinant IL-15	BioLegend	Cat# 566304

(*Continued on next page*)

Continued

REAGENT or RESOURCE	SOURCE	IDENTIFIER
PMA	Sigma-Aldrich	Cat# P1585
Ionomycin	Sigma-Aldrich	Cat# I9657
Monensin	Invitrogen	Cat# 00-4505-51
Brefeldin A	Invitrogen	Cat# 00-4506-51
Collagenase IV	Sigma	Cat# C5138
DNAse I	Roche	Cat# 11284932001
Percoll	Cytiva	Cat# 17089101
LIVE DEAD Fixable Blue stain	Invitrogen	Cat# L34962
Insulin	Novo Nordisk	Cat# GR7B338
D-(+)-Glucose	Sigma	Cat# G8270
TRITC Dextran	Sigma-Aldrich	Cat# T1287
FCS	Eurobio scientific	Cat# CVFSVF00-01
Opti-MEM + GlutaMAX	Gibco	Cat# 51985-026
TaqMan Universal PCR Master Mix	Applied Biosystems	Cat# 4304437
P/S	Gibco	Cat# 15070-063
2-mercaptoethanol	Gibco	Cat# 31350-010
Critical commercial assays		
FITC BrdU Flow Kit	BD Biosciences	Cat# 51-2354AK; RRID:AB_2617060
CellTrace Violet Cell Proliferation Kit	Invitrogen	Cat# C34557
Luminex Mouse Premixed Multi-Analyte Kit	R&D Systems	Cat#LXSAMSM-16
Mouse ProcartaPlex Mix&Match 13-plex	Invitrogen	Cat# PPX-13-MXZTE2Y
FITC Annexin V Apoptosis Detection Kit I	BD Biosciences	Cat# 556547; RRID:AB_2869082
PrimeScript RT Reagent Kit	Takara	Cat# RR037B
Nuclear Transcription Factor Buffer Set	BioLegend	Cat# 424401
RNEasy Micro kit	QIAGEN	Cat# 74004
Experimental models: Organisms/strains		
Mouse C57BL/6j	Jackson Laboratory	Strain #:000664; RRID:IMSR_JAX:000664
Mouse B6.129S6(Cg)-Spp1^{tm1Blh}/J	Jackson Laboratory	Strain #:004936; RRID:IMSR_JAX:004936
Mouse C57BL/6J-Myd88tm1Aki	Dr Laurent Debarbieux, Institut Pasteur, Paris, France	N/A
Mouse B6(Cg)-*Il15*$^{tm1.2Nsl}$/J	Jackson Laboratory	Strain #:034239; RRID:IMSR_JAX:034239
Mouse Ifng−/−	Dr Philippe Bousso, Institut Pasteur, Paris, France	N/A
Oligonucleotides		
Acta2	Applied Biosystems	Mm00725412_s1
Arg1	Applied Biosystems	Mm00475988_m1
Bcl2	Applied Biosystems	Mm00477631_m1
Ccl2	Applied Biosystems	Mm00441242_m1
Col1a1	Applied Biosystems	Mm00801666_g1
Cxcl9	Applied Biosystems	Mm00434946_m1
Cxcl11	Applied Biosystems	Mm00444662_m1
Cxcl10	Applied Biosystems	Mm00445235_m1
Cxcr3	Applied Biosystems	Mm99999054_s1
Eomes	Applied Biosystems	Mm01351984_m1
Il1b	Applied Biosystems	Mm00434228_m1
Il10	Applied Biosystems	Mm01288386_m1
Il15	Applied Biosystems	Mm00434210_m1
Il15Ra	Applied Biosystems	Mm04336046_m1

(*Continued on next page*)

Continued

REAGENT or RESOURCE	SOURCE	IDENTIFIER
Klf2	Applied Biosystems	Mm00500486_g1
Mcl1	Applied Biosystems	Mm01257351_g1
Prdm1	Applied Biosystems	Mm00476128_m1
Spp1	Applied Biosystems	Mm00436767_m1
Tbx21	Applied Biosystems	Mm00450960_m1
Timp1	Applied Biosystems	Mm01341361_m1
Tnf	Applied Biosystems	Mm00443258_m1
Software and algorithms		
FlowJo v10.9.0	FlowJo	https://www.flowjo.com/
GraphPad Prism 10	GraphPad	https://www.graphpad.com/
Rtsne R package	RDocumentation	https://www.rdocumentation.org/packages/Rtsne/versions/0.16/topics/Rtsne
ImageJ	ImageJ	https://ImageJ.nih.gov/ij/
Other		
Methionine- and choline-deficient (MCD) diet	ssniff-Spezialdiäten GmbH	TC 90.262
High Fat High Glucose (HFHG) diet	Safe	TD08811

RESOURCE AVAILABILITY

Lead contact

Further information and requests for resources and reagents should be directed to and will be fulfilled by the Lead Contact, Rachel GOLUB (rachel.golub@pasteur.fr).

Materials availability

This paper did not generate new unique reagents.

Data and code availability

- All data reported in this paper will be shared by the lead contact upon request.
- This paper does not report original code.
- Any additional information required to reanalyze the data reported in this work paper is available from the lead contact upon request.

EXPERIMENTAL MODEL AND STUDY PARTICIPANT DETAILS

In vivo animal studies

C57BL/6J mice were purchased from Envigo. IL-15 knockout (KO), IFNγ KO, Myd88 KO and OPN KO mice were bred in the animal facilities at Pasteur Institute, Paris. All mice were maintained under specific-pathogen-free conditions, air renewal (20 times per hour), constant ambient temperature of 22 $\pm$ 2°C and 14:10 h light–dark cycle. All mice used during diets were 8- to 10-week-old males at the beginning of the feeding. All experiments involving mice were performed according to guidelines issued by the Institut Pasteur Ethics Committee and were approved by the French Ministry of Research (projects nos. 02080.02, 02081.02, CETEA 2014-0058 and CETEA 2014-0059). Methionine- and choline-deficient (MCD) diet (ssniff-Spezialdiäten GmbH, TC 90.262) and High Fat High Glucose (HFHG) diet (Safe, TD08811) were used to induce non-alcoholic steatohepatitis in mice. The control mice were fed a Chow diet provided by the animal facility at Pasteur Institute.

METHOD DETAILS

Flow cytometry and cell sorting

All antibodies were purchased from BD Biosciences, eBioscience, BioLegend, Sony or R&D Systems. Antibodies were biotinylated or conjugated to fluorochromes [fluorescein isothiocyanate (FITC), phycoerythrin (PE), PECy5, PerCPCy5.5, PECy7, allophycocyanin (APC), Alexa Fluor 647, APCCy7, Pacific Blue, BV421, BV510, BV605, BV650, BV711, BV786, BUV395, BUV563 and BUV805] and were specific for the following mouse antigens: Ly76 (TER119), Gr-1 (RB6-8C5), CD3e (145-2C11), CD19 (6D5), NK1.1 (PK136), IL-7Ra (A7R34), CD8 (53-6.7), CD4 (RM4-5), Thy1.2 (53-2.1), NKp46 (29A1.4), IFNg (XMG1.2), CD45.2 (104), CD49a (HMa1), CD49b

(DX5), T-BET (4B10), EOMES (Dan11mag), BCL-2 (BCL/10C4), TNFa (MP6-XT22), CD11b (M1/70), CD11c (HL3), Granzyme B (GB12), F4/80 (BM8), MHCII (M5/114.15.2), CD226 (10E5), CD94 (18d3), NKG2A (16A11), NKG2D (CX5), Ly6C (HK1.4), Ly6G (1A8), CD45 (30-F11), CD122 (TM-b1), CD183 (CXCR3-173), CD27 (LG.3A10), CD51 (RMV-7), CD44 (IM-7). BrdU and purified OPN were purchased from R&D. Flow cytometry data were acquired using a Symphony A5 flow cytometer (BD Biosciences) and analyzed with FlowJo software (FlowJo 10.6.1 Tree Star).

For intracellular staining of transcription factors, cells were fixed and permeabilized with True Nuclear Transcription Factor Buffer Set (BioLegend). For intracellular cytokine staining, cells were re-stimulated for 5-6h at 37°C in Opti-MEM medium (Gibco) containing 10% fetal calf serum (FCS) (Eurobio), 1% Penicillin/Streptomycin (Gibco) with PMA (Sigma-Aldrich, 30 ng/mL) and Ionomycin (Sigma-Aldrich, 500 ng/mL) in the presence of Monensin and Brefeldin A (Invitrogen, 1:1000 dilution), followed by staining with fixation/permeabilization. For cell cycle analysis, cells were stained with an anti-Ki67 antibody (B56) after fixation and incubated with DAPI solution during 10 min at room temperature after permeabilization.

For BrdU assays, mice received a single intravenous injection of 1 mg of BrdU for 6g of body weight. Twelve hours later, the mice were sacrificed, single-cell suspensions were obtained from the BM and the lineage-negative fractions were stained for NK cells and progenitors. Cells were fixed and stained for BrdU using the FITC-BrdU Flow Kit (BD Biosciences) according to manufacturer's protocol.

For cell sorting, a FACSAria III (BD Biosciences) was used to purify subset of stained immune cells. Purity of sorted cells was above 80%.

Tissue dissociation

Spleens were harvested, dissociated, and resuspended in Hanks' balanced salt solution (HBSS) (Gibco) supplemented with 2% FCS (Gibco). Livers were flushed with 5 mL of cold Phosphate Buffered Saline solution (PBS) (Gibco) and harvested. After being cut in small fragments, livers were incubated in RPMI medium (Gibco) plus collagenase IV (Sigma-Aldrich, C5138, 0.25 mg/mL) and DNAse I (Roche, 50 μg/mL) during 45 min at 37°C and 5% CO2 under shaking. Livers were centrifuged at 370g for 7 min, the supernatant was eliminated, and the pellet resuspended in HBSS supplemented with 2% FCS. Cells were collected by centrifugation (370g, 7 min) and resuspended in 44% solution of Percoll (Cytiva). After centrifugation at 600*g* for 20 min the cell pellet was washed and resuspended in HBSS containing 2% FCS. BM was isolated by flushing the femur and tibia with 200 μL of HBSS. After centrifugation (370g, 7 min) the supernatant was collected for protein titration and the pellet was resuspended in HBSS containing 2% FCS. Red blood cells were lysed by 1 min-incubation with Ammonium-Chlorure-Potassium (ACK) solution (Gibco). BM cells were stained with biotin-labelled antibodies against lineage markers (Ly76, GR-1, CD19, CD3, CD4 and CD8), incubated with Anti-Biotin Microbeads (Miltenyi Biotec) during 15 min and magnetically depleted of Lin^+ cells via the use of LS MACS columns (Miltenyi Biotec). Blood was harvested using a 1mL syringe (BD Plastipak) and laid on Ficoll Paque Plus (GE Healthcare). After centrifugation at 600*g* for 20 min at 20°C, cells at the interface were washed and recovered in 2% FCS HBSS.

Co-culture assay

WT, OPN-deficient or IL-15-deficient BM $Ly6C^{low}$ monocytes and $CD27^+CD11b^-$ BM NK cells were FACS-sorted and were plated at a 10:1 ratio (20,000 monocytes for 2,000 NK cells per well) in Opti-MEM medium, 10% FCS, 1% Penicillin/Streptomycin supplemented with recombinant mouse IL-15 (10 ng/mL, BioLegend) and in one condition supplemented with recombinant mouse OPN (50 ng/mL, R&D systems). The cells were co-cultured during 3 or 5 days at 37°C and 5% CO2 before being stained for analysis. Single cultures with 2,000 NK cells per well were used as controls for the co-culture conditions.

Cell culture and apoptosis assays

FACS-sorted BM $Ly6C^{low}$ monocytes were plated at a concentration of 150 000 cells/ml in Opti-MEM medium (Gibco) containing 10% fetal calf serum (FCS) (eurobio), 1% Penicillin/Streptomycin (Gibco) alone or with 5% of M-CSF or with recombinant mouse OPN (5 μg/mL, R&D systems). Incucyte Annexin V near-infrared (NIR) dye (4768, Sartorius) was added to the medium. Cells were cultured for 3 days at 37°C and 5% CO2. An Incucyte SX5 was used to measure and record the level of fluorescence of each well every 3 h.

FACS-sorted $CD27^+CD11b^-$ NK cells were plated at a concentration of 150 000 cells/ml in Opti-MEM medium (Gibco) containing 10% fetal calf serum (FCS) (eurobio), 1% Penicillin/Streptomycin (Gibco) with recombinant mouse IL-15 (10 ng/mL, BioLegend) supplemented or not with recombinant mouse OPN (50 ng/mL, R&D systems). After a 5-day culture, the cells were harvested and stained for analysis. NK cell survival was assessed using the FITC Annexin V Apoptosis Detection Kit (BD Bioscience) according to manufacturer's instructions.

Cell proliferation assay

Cell proliferation of NK cells in a co-culture assay was measured after 3 days using the CellTrace Violet Cell Proliferation Kit following the manufacturer's protocol. Briefly, $CD27^+CD11b^-$ NK cells were FACS-sorted and incubated with a CellTrace Violet staining solution at 2.5 μM for 20 min at 37°C. Pure FCS was added to the solution to capture unbound dye. After a 5-min incubation, NK cells were washed and resuspended in culture medium with IL-15 (10 ng/mL, BioLegend) and were either cultured alone or co-cultured with WT or IL-15 KO BM $Ly6C^{low}$ monocytes for 3 days.

NK cell depletion

Each mouse was injected intraperitoneally with 50 μg of anti-asialo GM1 antibody (Invitrogen, 16-6507-39) for NK cells depletion three days before the start of the MCD diet. The injection was repeated twice a week during the four weeks of diet.

Quantification of proteins

Protein levels in culture supernatants and BM supernatants were measured using the Luminex Mouse Magnetic Assay (R&D Systems) and the PROCARTAPLEX kit (Life Technologies) according to manufacturer's instructions. Data was obtained with a Bio-Plex 200 device (Luminex).

RNA extraction and RT-qPCR

Total RNA was extracted from FACS-purified cells or from liver tissue using respectively the RNeasy Micro and Mini Kits (Qiagen) according to manufacturer's protocol. Complementary DNA (cDNA) was obtained with the PrimeScript RT Reagent Kit (Takara). A 7300 Real-Time PCR System (Applied Biosystems) and TaqMan technology (Applied Biosystems by ThermoFisher Scientific) were used for qRT-PCR analysis. All TaqMan primers were purchased from ThermoFisher Scientific: Acta2 (Mm00725412_s1), Arg1 (Mm00475988_m1), Bcl2 (Mm00477631_m1), Ccl2 (Mm00441242_m1), Col1a1 (Mm00801666_g1), Cxcl9 (Mm00434946_m1), Cxcl11 (Mm00444662_m1), Cxcl10 (Mm00445235_m1), Cxcr3 (Mm99999054_s1), Eomes (Mm01351984_m1), Il1b (Mm00434228_m1), Il10 (Mm01288386_m1), Il15 (Mm00434210_m1), Il15Ra (Mm04336046_m1), Klf2 (Mm00500486_g1), Mcl1 (Mm01257351_g1), Prdm1 (Mm00476128_m1), Spp1 (Mm00436767_m1), Tbx21 (Mm00450960_m1), Timp1 (Mm01341361_m1), Tnf (Mm00443258_m1).

Biochemical analysis

Serum ALAT/ASAT, cholesterol and triglycerides levels were determined using a multiparametric Olympus AU 400 automat (Beckman Coulter) at the Laboratoire de biochimie, Institut Claude Bernard, Paris.

Histology

Liver tissue was fixed in 10% buffered formalin, embedded in paraffin, sectioned, and stained with either hematoxylin and eosin (HE) or F4/80 antibody at the Histology Department of Pasteur Institute, Paris. For Oil Red'O staining, liver tissue was frozen in liquid nitrogen prior to be sectioned and stained. Samples were then scanned and analyzed using software Fiji (ImageJ).

Oral glucose tolerance test (OGTT) and Insuline tolerance test (ITT)

To perform OGTT, mice were fasted overnight. Basal blood glucose level was determined for each mouse prior to oral gavage with D-(+)-Glucose (2 mg per g of mouse body weight, Sigma-Aldrich). A small cut at the tip of the mouse's tail was made to obtain drops of blood which were collected on test strips (ACCU-CHEK, Roche) then inserted into a smart view blood glucose monitor (ACCU-CHEK, Roche) to analyze blood glucose levels. Measurements were made at times −10, 0, 15, 30, 60, 90 and 120 min with time 0 being the glucose gavage (.

To perform ITT, mice were fasted 4–6 h prior to intraperitoneal (IP) insulin injection (0.0005 U per g of mouse body weight, Insulin (Novo Nordisk). The blood glucose levels were measured the same way as for the OGTT at the times 0, 10, 15, 30, 60, 90, 120 min with time 0 being the IP insulin injection.

Intestinal paracellular permeability test

TRITC-dextran (Sigma-Aldrich, T1287) was administered by gavage to 6-h-fasted-mice (600 mg per kg of body weight). At time 0 (which corresponds to immediately after gavage) as well as 1h, 3h and 5h post-gavage, blood was collected from the tip of the tail vein (40μL) into EDTA-coated tubes and centrifuged (4°C, 2 000 g for 10 min). Plasma was diluted 1:10 (v/v) in PBS and the TRITC-dextran concentration was determined using a fluorescence spectrophotometer (Fluostar; SLT, Crailsheim, Germany) at 485 nm excitation and 535 nm emission wavelengths. Standard curves were obtained by diluting TRITC-dextran solution in plasma from non-treated mice diluted in PBS (1:10 v/v).

BM reconstitution

8-week-old Rag2$^{-/-}\gamma c^{-/-}$ mice were sub-lethally irradiated (4 Gy) at the Pasteur Institute and received a 1:1 mixture of 10 million BM cells from C57Bl/6 and Kaede mice that were previously fed respectively with Chow and MCD diet for 4 weeks. The transplantation was performed via retroorbital injection while anesthetized with ketamine/xylazine. The recipients were then put under Chow or MCD diet and sacrificed after 4 weeks. BM and livers were collected and analyzed for donor frequencies by flow cytometry.

QUANTIFICATION AND STATISTICAL ANALYSIS

Bioinformatics

t-SNE representation: For visualisation, the dimensionality of the datasets was further reduced using the "Barnes-hut" approximate version of t-SNE. This was implemented using the Rtsne function from the Rtsne R package using 800 iterations and a perplexity

setting that varied from 10 to 30 depending on the size of the dataset. Phenograph takes as input a matrix of N single-cell measurements and partitions them into subpopulations by clustering a graph that represents their phenotypic similarity.

Statistical analysis

Statistical analysis was performed with the Mann-Whitney nonparametric test where appropriate. These tests were performed using Prism software (GraphPad). Graphs containing error bars show means +/SD. Statistical significance is represented as follows: *$p < 0.05$, **$p < 0.01$ and ***$p < 0.001$.